

Entropy in self-assembly

FRANCESCO SCIORTINO

Sapienza Università di Roma - Piazzale Aldo Moro 5, I-00185, Italy

received 1 July 2019

Summary. — Colloidal systems show beautiful examples of how entropy can lead to self-assembly of ordered structures, challenging our perception of disorder. In fact, dispersion of hard colloidal particles, systems in which by default entropy is the only thermodynamic driving force, displays both translational and orientational order on increasing density. Entropy is also a fundamental concept for describing effective interactions between colloidal particles. In several cases, entropy maximization generates strong attractive forces, capable of inducing condensation and sometimes crystallization. These entropic forces can even be exploited to drive colloids in specific locations or to orient them in the build-up of supracolloidal aggregates. Depletion interactions and combinatorial contributions are two important manifestations of these forces. Entropy also plays a leading role in systems exploring the bottom of their potential energy surface. In patchy colloids, particles interacting with highly anisotropic and localized potentials, ground-state structures are often degenerate in energy, leaving entropy to decide the thermodynamically stable polymorph. A striking result is the possibility of generating colloidal “liquids” thermodynamically more stable than colloidal “crystals” even at vanishing temperature.

512	1.	Introduction
513	2.	The classical cases
513	2'1.	Phase transition in hard spheres
516	2'2.	Phase transition in hard disks
516	2'3.	Nematic ordering in hard cylinders
520	2'4.	Dense hard-bodies phases
521	3.	Entropy in the ground state
521	3'1.	Patchy colloids: sampling the ground state
522	3'2.	Liquid or crystal again: the role of bond flexibility
524	3'3.	Entropy selection of the stable crystals
525	3'4.	Vitrimers: entropy-driven dynamics in the ground state
528	4.	Entropy attracts
528	4'1.	Depletion interactions
531	4'2.	Entropic effective potential: from two dimensions to quasi-two dimensions

532	4.3.	Combinatorial entropy: microemulsion droplets linked by telechelic polymers
534	4.4.	Combinatorial entropy: DNA grafted particles
536	4.5.	Combinatorial entropy: superselectivity
537	5.	Equilibrium clustering
539	6.	When entropy competes with energy
539	6.1.	Dipolar hard spheres
541	6.2.	Competing patches
542	6.3.	Janus
542	6.4.	Re-entrant gels
544	7.	Conclusions

1. – Introduction

Entropy plays a very important role in soft-matter self-assembly, the process by which information encoded in the size and shape of the constituent particles produces mesoscopic and macroscopic ordered states. Oppositely to the common-sense description of entropy as a disordering agent, in a large variety of systems entropy constitutes the only driving force for ordering. Some of these cases will be discussed in this article.

The focus of this review are colloidal dispersions, particles of nanometric or micrometric size dispersed in solution. The upper limit to the particle size is fixed by the requirement that the thermal energy ($k_B T$) is able to compensate for gravitational sedimentation. Equilibrium statistical mechanics then provides a valuable framework for predicting the collective behavior of the system.

The review begins (sect. 2) by discussing two classic soft-matter cases in which entropy plays a fundamental role in ordering, specifically hard-sphere (and hard disk) crystallization [1] and nematic ordering in elongated hard particles [2]. In these two cases, the role of entropy is crystal clear, since by definition particles interact only via excluded volume. In fact, the interaction potential is infinite if two particles overlap and zero elsewhere, so that by construction energy does not play any role. The only relevant configurations are the ones without particle-particle overlaps, and all of them are equally probable. For each packing fraction, the volume in phase-space associated to ordered, partially ordered, or disordered states is the quantity that decides the thermodynamic most stable phase. An ordered state either orientational (nematic) or translational (crystallization) can arise from the maximization of such a volume.

Today, colloidal particles can be engineered with sophisticated inter-particle interaction potentials, including attractive directional interactions [3-9]. A large variety of colloidal particles with functionalized surfaces have been synthesised and shown to be able to self-assemble in quite interesting structures, not all of them mimicking the ones found in molecular systems. In some cases, the surface patterning is such that only localized regions of the surface (patches) are able to bind with other particles, providing valence to colloids. Patchy colloids [10, 11, 6, 12-14], soft patchy micelles [15], DNA patchy particles [16, 17] as well as some proteins [18-21] are important examples of this category. These anisotropically interacting particles can bind to each other, reaching sometimes states in which all possible patches are bonded. In this case, the energetic driving force is fundamental in reaching the fully bonded ground state. But which of all possible fully bonded structures is the thermodynamically stable one is decided by

entropy (sect. 3). Thus patchy colloids, being able to explore their ground state at low temperatures, exploit once more entropy as the main driving force for self-assembly.

The important role that entropy plays in soft-matter systems is often expressed in terms of an effective particle-particle interaction potential. Differently from atoms and molecules, colloidal particles interact via forces arising from a restricted thermodynamic averaging of elementary interactions [22]. These effective forces, even at the two-body level, include by construction an entropic part, being a Boltzmann-weighted average of all phase-space points consistent with a fixed inter-particle distance and relative orientation. In some cases, the effective force is completely entropic in origin but still can induce strong particle-particle aggregation. The depletion interaction [23-25], arising when large colloidal particles are immersed in a bath of smaller cosolutes, is the classic example of this class of entropic effective potentials. Since their discovery, depletion interactions have been progressively mastered to exploit particle and cosolute shape [26-28,13] (including positive and negative curvature cases), particle roughness [29], cosolute aggregation [30,31]. Another important class of entropy-driven effective potentials originates from combinatorial contributions [32], a phenomenon amplified by the possibility exploited by specific colloidal particles to equivalently give rise to intra- or inter-particle bonding. Depletion interactions and colloidal association driven by combinatorial contributions are reviewed in sect. 4. The discussion of few soft-matter cases in which entropy and energy compete in the self-assembly process, resulting in systems in which the structural and dynamic properties are strongly sensitive to temperature or pressure, concludes the review.

It would be unfair not to mention that quite a few interesting entropy-controlled phenomena of soft-matter relevance are found in polymer physics [33]. Those are not discussed here. The interested reader can consult refs. [34,35]. Finally, I also recommend two beautiful reviews related to this work by Daan Frenkel [36] and Fernandez Escobedo [37] as well as the stimulating book by Roberto Piazza [38].

2. – The classical cases

2.1. Phase transition in hard spheres. – In January 1957 in New Jersey during a symposium on many-body problems, Alder and Wainwright presented their first results on molecular dynamics simulations of hard spheres (HS), suggesting the possibility of a transition toward an ordered crystalline phase on increasing the density of the HS fluid [1]. George Uhlenbeck, during the discussion time, asked the participants to express their personal feeling on such a possibility and the vote ended up even [39]. The cartoon in fig. 1(b) and the commonly but improperly assumed connection between entropy and disorder possibly explain the difficulty of reaching a consensus on this question. Hard spheres interact only via excluded volume, preventing any pair of particles from becoming closer than their diameters (fig. 1(a)). No energy is involved in the interaction. Thus, thermodynamic is fully controlled by the entropic term in the free energy. Improperly, the possibility of hard-sphere crystallization was perceived as contradicting the meaning of entropy as a driving force toward increasing disorder. How can a crystal be more disordered than a fluid configuration?

To properly answer the question, one needs to consider the number of microstates explored in the fluid and in the crystal phase. In the crystal, particles move in cages provided by their own neighbours, as vividly shown in the cathode-ray tube used by Alder and Wainwright to visualize the molecular dynamics trajectories of two-dimensional crystalline hard disks (fig. 1(d)). The width of the spots created by the bright line

paths is a visual measure of the phase-space sampled by each particle. The log of the number of sampled microstates constitutes the entropy of the crystal, which we can name vibrational or cage entropy. In the fluid, we can distinguish two contributions to the entropy: a vibrational contribution, which again depends on the available volume inside the cage and a second contribution which measures the number of different disordered arrangements of the particles, commonly named as configurational entropy. The mean square displacement (MSD) of a particle in the dense fluid or in the crystal can be considered as a proxy for the vibrational contribution to entropy. Figure 1(e) contrasts the MSD in disordered and ordered dense HS configurations to provide evidence that the phase-space volume explored by the particles in the cage (vibrational motion) is significantly smaller in disordered configurations. The difference in vibrational entropy can be so large that the additional configurational contribution is not any longer sufficient to thermodynamically stabilise the fluid phase. The ordered crystal has a larger entropy than the fluid.

Quite accurate estimates of the HS entropy are nowadays available. The fluid phase entropy per particle can be approximated with the Carnahan-Starling (CS) expression [41] (slightly more accurate expressions than the one by Kolafa —first appeared as eq. (4.46) in [42]— are available)

$$(1) \quad \frac{S_{\text{ex}}^{\text{CS}}}{k_{\text{B}}} = -\frac{4\phi - 3\phi^2}{(1 - \phi)^2},$$

where ϕ is the packing fraction. The face-centered-cubic (FCC) crystal free energy can be approximated using Hall expression [43], a phenomenological expression based on computer simulation results. Hall noted that the compressibility factor Z_{HS} of the FCC HS crystal can be quite accurately modelled by

$$(2) \quad Z_{\text{HS}} = \frac{\beta P}{\rho} = \frac{1 + \phi + \phi^2 - 0.67825\phi^3 - \phi^4 - 0.5\phi^5 - 6.028\phi^6 f(\phi)}{1 - 3\phi + 3\phi^2 - 1.004305\phi^3},$$

with $f(\phi) = \exp((\pi\sqrt{2}/6 - \phi)[7.9 - 3.9(\pi\sqrt{2}/6 - \phi)])$. In order to calculate the excess entropy S^{ex} per particle from the compressibility factor Z_{HS} , a thermodynamic integration in ϕ can be performed, obtaining

$$(3) \quad \frac{S^{\text{ex}}(\phi)}{k_{\text{B}}} = \frac{S^{\text{ex}}(\phi^*)}{k_{\text{B}}} - \int_{\phi^*}^{\phi} \left(\frac{\beta P}{\rho} - 1 \right) \frac{d\phi'}{\phi'}.$$

The integration in eq. (3) is usually started from $\phi^* = 0.544993$, a value for which an accurate estimate of the excess crystal entropy $\frac{S^{\text{ex}}(\phi^*)}{k_{\text{B}}} = -5.91889$ based on computer simulation is available [44].

Figure 1(h) shows the fluid and crystal entropy per particle as a function of the volume per particle for the HS system. In the case of hard bodies, the free energy F has only the entropic contribution $F = -TS$. Thus the pressure, the volume derivative of the free energy, is $P = T\partial S/\partial V|_T$. The pressure is thus nothing more than the derivative of the entropy function reported in fig. 1(h). Hence, the common tangent line shown in fig. 1(h) identifies two phases (fluid and crystal) with the same T , P and identical chemical potential μ (being $\mu = (F + PV)/N$, see caption of fig. 1). The equality of T , P and μ sets the condition for phase coexistence. In the region between the two

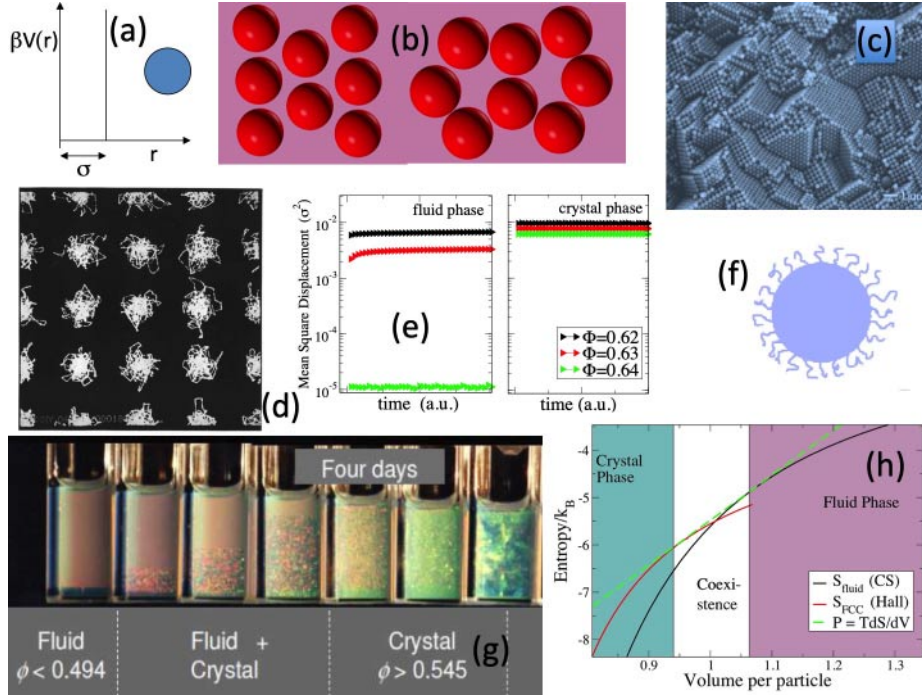


Fig. 1. – The hard-sphere model. (a) The radial dependence of the interaction potential, $\beta V(r)$. The potential is infinite for r smaller than the particle diameter and zero everywhere else. (b) A cartoon of a crystalline and of a fluid configuration to highlight the different order perceived by our eyes, trained to capture only the configurational part of the entropy. (c) An electron microscope image of a colloidal crystal (courtesy of D. Pine). The particles in the photograph are made from polystyrene, a common commercial plastic. Notice that there are both hexagonal and square planes visible, which is consistent with a face-centered cubic lattice. (d) The original trajectories detected in the first molecular dynamics calculation of hard disks [1] as shown by the cathode-ray tube used by Alder and Wainwright (redrawn from ref. [1]). (e) A comparison between the mean square displacement of HS particles in the fluid and in the crystal phase. In the crystal phase, particles rattle in larger cages, a confirmation of the larger vibrational entropy. (f) A cartoon of a polymer-grafted colloid. (g) The fluid, coexisting and crystal phases observed in the classic experiment by Pusey and van Meegen [40] (Courtesy of P. Pusey). (h) The volume dependence of the fluid and crystal entropy (with an arbitrary additive constant) as predicted by the CS and the Hall equation of state. The dashed line is tangent to both the fluid and the crystal entropy. Since $P = T dS/dV$, the two tangent points indicate two volumes V_{xt} and V_{fluid} for which both temperature and pressure are identical. If we further indicate with S_0 the intercept of the same line at zero volume, then we can write for these two points $S = S_0 + V dS/dV = S_0 + PV/T$. Then the Gibbs free energy per particle $G/N = (-TS + PV)/N$ is equal to $-TS_0/N$ for both V_{xt} and V_{fluid} , proving that these two volumes have also the same chemical potential $\mu \equiv G/N$. Thus, V_{xt} and V_{fluid} are two coexisting phases.

coexisting phases, in the thermodynamic limit, entropy is maximised by the presence of two coexisting phases.

Despite common jokes suggest that most objects in the physicist's mind are hard spheres, the laboratory realisation of a HS model has been delayed by the difficulties of synthesise quite monodisperse colloidal particles with negligible electrostatic and van

der Waals attractions. To experimentally realize the ideal HS potential one needs to suppress the inevitable van der Waals (short-range) interaction originating from the particle polarizability [45]. The colloids are chemically treated, for example via steric stabilization, to prevent close approach. To further reduce the effect of van der Waals interactions (and increase the transparency of the sample) particles are dispersed in a solvent of comparable refractive index. Steric stabilization requires the grafting of polymer chains on the surface of the colloidal particle (fig. 1(f)). Similarly, a density match between solvent and colloidal particles helps to minimize the effect of gravity. One of the most studied model systems is composed of poly-(methyl methacrylate) (PMMA) particles, grafted with a layer of poly-(12-hydroxy stearic acid) (PHSA) in a solvent composed of decalin and tetralin. The measured equation of state does not deviate from the one of a perfect HS system under any relevant experimental condition [46], for particle sizes larger than 50 nm in diameter and for packing fractions as large as 0.64. An ingenious measurement of the equation of state for HS colloids is possible by detecting the equilibrium sedimentation profile resulting from the presence of the Earth gravitational field [47]. Figure 1(g) shows one of the first experimental evidences of HS crystallisation (and glass formation) in the laboratory [40].

2.2. Phase transition in hard disks. – The phase behavior of hard disks (HD), the two-dimension (2-d) counterpart of the hard-sphere system, is particularly interesting. Controversies concerning the nature of HD crystallization process have persisted for decades. Its investigation stimulated the development of numerical methodologies (including the first Monte Carlo [48] and Molecular Dynamics calculations [49]). Recent numerical results, based on the event-chain Monte Carlo algorithm (ECMC) [50], supported by experimental evidence [51], have shown that the crystallization scenarios in HD are more complex than previously thought. On increasing surface fraction, the isotropic fluid transforms via a first-order fluid-hexatic transition to an intermediate phase [52]. The hexatic phase is characterized by sixfold orientational order which extends over (quasi-)long range, while the positional order is short-ranged. It is this intermediate phase that, upon further increase of the density, gives then rise to a continuous hexatic-solid transition. The fluid then transforms into a solid through an intermediate hexatic phase. The existence of an intermediate phase is not consistent with the standard Kosterlitz-Thouless-Halperin-Nelson-Young (KTHNY) scenario [53,54], predicting a continuous transition both from the fluid to the hexatic and from the hexatic to the solid. It also differs from other first-order liquid-solid transition scenarios, which exhibit no intermediate hexatic phase (see ref. [55] and references therein).

Recent calculations [56] on binary HD mixtures have shown that the stability window of the hexatic phase progressively shrinks on increasing the concentration of small disks until the line of continuous transitions terminates at an end point beyond which melting becomes a first-order liquid-solid transition. The surprisingly low concentrations of small disks at the end point (less than 1%), emphasizes the fragility of the hexatic phase with respect to disorder in the particles diameter.

2.3. Nematic ordering in hard cylinders. – While HS crystallisation, in two and three dimensions, shows the power of the entropy associated to particle center-of-mass position, the nematic transition provides evidence of the important entropic contributions arising from particle orientation. Interestingly, the possibility that entropy could act as an ordering force was already evident in Onsager's theory on the effect of shape in colloidal solutions [2], a contribution which appeared in the *Annales of the New York Academy of*

Science already in 1949, several years before the debate on hard-sphere crystallization.

Let us assume that particles can be considered distinct according to the orientation of their principal axis \mathbf{a} . The idea is to write the configurational part of the partition function $Z_{ig}(V)$ of an ideal gas of particles oriented according to some pre-defined distribution $\{N_i\}$, where N_i is the number of particles oriented in the solid angle $\Delta\Omega_i$. If the $\{N_i\}$ are chosen to be equally probable (isotropic distribution of orientations), then $\ln Z_{ig}(V)$ will provide the appropriate free energy (the entropy) of the isotropic phase. If the $\{N_i\}$ are chosen in such a way that one particular orientation is preferred, then the calculated $\ln Z_{ig}(V)$ will provide the entropy of the nematic phase described by $\{N_i\}$. This exercise can be repeated for several $\{N_i\}$ distributions to identify the most probable one (the one with the highest entropy). By comparing the entropy of the isotropic phase and the entropy of the most disordered nematic phase, Onsager predicted the existence of a first-order phase transition.

For a set of orientations $\{N_i\}$, $Z_{ig}(V)$ can be written as (setting the thermal wavelength as unit of length)

$$(4) \quad Z_{ig}(V) = \prod_i \frac{1}{N_i!} \left[\frac{\Delta\Omega_i}{4\pi} \int d\mathbf{r} \right]^{N_i},$$

corresponding, using Stirling's approximation, to an entropy $S(V) \equiv k_B \ln Z(V)$

$$(5) \quad \frac{S_{ig}(V)}{k_B} = \sum_i N_i \left[1 + \ln \left(\frac{V \Delta\Omega_i}{4\pi N_i} \right) \right].$$

If we add the virial contribution, therefore going beyond the ideal gas approximation, we obtain

$$(6) \quad \frac{S(V)}{k_B} = \sum_i N_i \left[1 + \ln \left(\frac{V \Delta\Omega_i}{4\pi N_i} \right) \right] + \frac{1}{2V} \sum_{i,j} \beta(\mathbf{a}_i, \mathbf{a}_j) N_i N_j,$$

where $-\beta(\mathbf{a}_i, \mathbf{a}_j)/2$ is the virial coefficient (the excluded volume) between two particles oriented as \mathbf{a}_i and \mathbf{a}_j . The virial contribution is strongly dependent on the relative orientation of the two particles, as shown in fig. 2(a-b). Parallel cylinders can be packed much more efficiently than perpendicular cylinders.

For cylinders of length L and diameter D , indicating with γ the angle between \mathbf{a}_i and \mathbf{a}_j [2]

$$(7) \quad -\beta(\gamma) = \frac{\pi}{2} D^3 \sin \gamma + \frac{\pi}{2} L D^2 + \frac{\pi}{2} L D^2 |\cos \gamma| + 2 L D^2 E(\sin \gamma) + 2 L^2 D \sin \gamma,$$

where

$$(8) \quad E(\sin \gamma) = \int_0^{\frac{\pi}{2}} (1 - \sin^2 \gamma \sin^2 \phi)^{1/2} d\phi.$$

In the limit of elongated particles, $L \gg D$,

$$(9) \quad \beta(\gamma) = -2 L^2 D |\sin \gamma|.$$

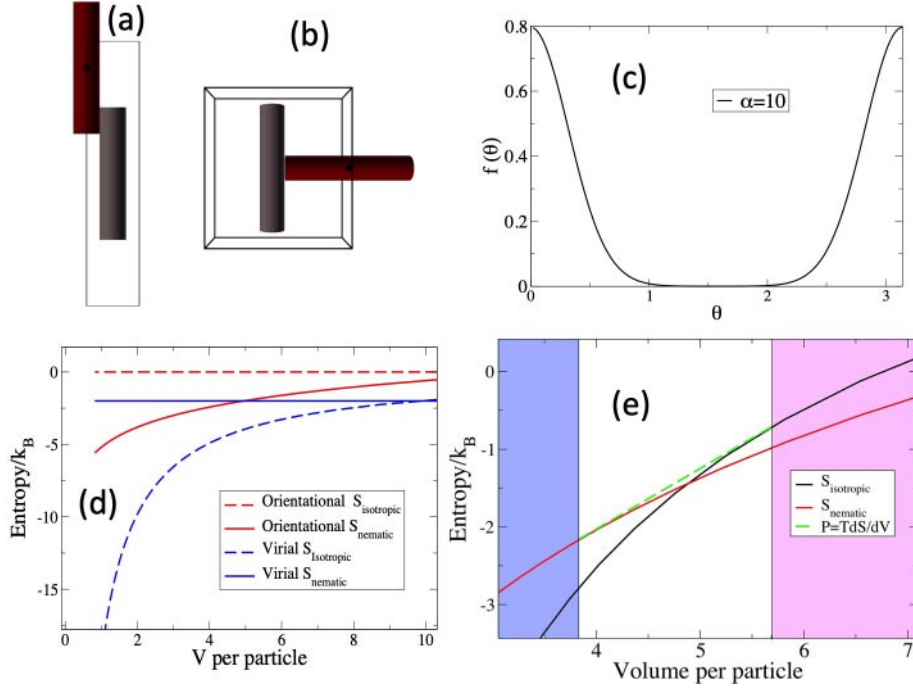


Fig. 2. – Isotropic-nematic phase for hard cylinders. (a) Excluded volume between two coaxial cylinders. The center of mass of the red cylinder can not explore the volume $\pi D^2 L$, where D is the diameter and L the length. (b) Excluded volume between two perpendicular cylinders. The center of mass of the red cylinder can not explore the volume $\approx 2DL^2$. (c) The functional form for the probability of orientation θ with respect to the nematic vector selected by Onsager for the case $\alpha = 10$. (d) The volume V dependence of the different entropic contributions. (e) The entropy of the isotropic and of the nematic phase calculated according to the Onsager theory for cylinders of diameter $D = 1$ and $L = 5$. The dashed line is tangent to both the isotropic and the nematic entropy. Hence, since $P = T dS/dV$, the two tangent points indicate two volumes $V_{\text{isotropic}}$ and V_{nematic} for which temperature, pressure, and chemical potential are identical.

Hence, in this limit, parallel cylinders do not exclude volume ($|\sin \gamma| = 0$), while perpendicular ones exclude the largest possible volume $2L^2 D$.

To evaluate $S(V)$ it is convenient to express N_i as $N_i = N f(\mathbf{a}) \Delta\Omega$ such that $f(\mathbf{a})$ becomes the probability of observing a particle oriented in the solid angle $\Delta\Omega$ centered around \mathbf{a} . Naturally,

$$(10) \quad \int f(\mathbf{a}) d\Omega = 1.$$

In the isotropic phase all orientations are equally probable and $f(\mathbf{a}) = \frac{1}{4\pi}$.

In the nematic phase we do not know *a priori* $f(\mathbf{a})$. As commonly done by physicists, Onsager postulated a reasonable functional form for $f(\mathbf{a})$ based on a free parameter α , a form for which he was able to solve all integrals requested in the calculation of $S(V)$. The parameter α was then evaluated as the one that maximizes the resulting nematic entropy.

The functional form chosen by Onsager was based on the physical intuition that in the nematic phase all particles are essentially oriented around the nematic direction (as in matches or spaghetti in their boxes). $f(\mathbf{a})$ should then be peaked around $\theta = 0$ and $\theta = \pi$, indicating with θ the angle between \mathbf{a} and the nematic direction. For mathematical convenience he chose the function

$$(11) \quad f(\theta) = \left(\frac{\alpha}{4\pi \sinh \alpha} \right) \cosh(\alpha \cos \theta),$$

whose angle dependence is reproduced in fig. 2(c). In the limit of $\alpha \gg 1$ this functional form is indeed peaked around $\theta = 0$ and $\theta = \pi$.

The entropy at the ideal gas level, for either the isotropic or the nematic phase is

$$(12) \quad \begin{aligned} \frac{S_{ig}(V)}{k_B} &= \sum_i N_i \left[1 + \ln \left(\frac{V \Delta \Omega_i}{4\pi N_i} \right) \right] \\ &= N \left[1 + \ln \left(\frac{V}{N} \right) \right] - N \int f(\mathbf{a}) \ln (4\pi f(\mathbf{a})) \, d\Omega. \end{aligned}$$

The first contribution is the entropy associated to the center of mass of the particles, the standard ideal-gas contribution. The second contribution depends only on the distribution of orientations and defines the orientational entropy of the system.

In the isotropic case, the orientational contribution vanishes since $f(\mathbf{a}) = \frac{1}{4\pi}$ and

$$(13) \quad \int f(\mathbf{a}) \ln [4\pi f(\mathbf{a})] \, d\Omega = 0.$$

In the nematic phase the ideal-gas orientational entropy is not zero. For the functional form postulated by Onsager (eq. (11)) the orientational entropy can be calculated for large α resulting in

$$(14) \quad \int f(\mathbf{a}) \ln (4\pi f(\mathbf{a})) \, d\Omega \approx \log \alpha - 1.$$

This contribution diverges to minus infinity on growing α , as expected by localization in classical physics.

The entropy associated to the excluded volume of course depends on the inter-particle orientation. Figure 2(a-b) shows the different excluded volume between pairs of cylinders perpendicularly or parallelely oriented. For the isotropic case, always in the limit $L \gg D$, (using $\int_0^\pi \sin^2 \gamma \, d\gamma = \pi/2$ and $\int_0^{2\pi} d\phi = 2\pi$) the virial contribution to entropy can be expressed as

$$(15) \quad \begin{aligned} \sum_{i,j} \beta(\mathbf{a}_i, \mathbf{a}_j) N_i N_j &= 2L^2 D \iint \beta(\gamma) \frac{N^2}{(4\pi)^2} \, d\Omega \, d\Omega' \\ &= N^2 \frac{1}{4\pi} \int \beta(\gamma) \sin \gamma \, d\gamma \, d\phi = -\frac{\pi}{2} L^2 D N^2. \end{aligned}$$

The corresponding expression for the nematic case (see Onsager article) is

$$(16) \quad \sum_{i,j} \beta(\mathbf{a}_i, \mathbf{a}_j) N_i N_j = N^2 \int \beta(\gamma) f(\Omega) f(\Omega') \sin \gamma \, d\gamma \, d\phi \approx -2L^2 D N^2 \sqrt{\frac{\pi}{\alpha}},$$

which approaches zero for large values of α .

For each value of α , Onsager was then able to estimate the system entropy. By taking the derivative of the nematic entropy with respect to α and equating it to zero, he was also able to evaluate the value α_{\max} for which the total entropy, sum of the ideal gas and of the virial term, is largest. Substitution of α_{\max} in eq. (16) and eq. (14) provides the best approximation (based on the selected functional form eq. (11)) to the nematic free energy.

Figure 2(d) shows, for cylinders with $L = 5$ and $D = 1$, the orientational and virial contributions to the entropy. A significant volume dependence of the entropy is present in the virial component of the isotropic phase (due to the change in the available volume accessible to the center of mass) and in the orientational component of the nematic phase (due to progressive reduction of the particle orientation).

The resulting final expressions for the entropy in the isotropic and nematic phase as predicted by the Onsager theory for cylinders are (defining $\rho = N/V$)

$$(17) \quad S_{\text{iso}}^{\text{Onsager}} = N \left[1 - \ln(\rho) - \rho \frac{\pi L^2 D}{4} \right]$$

and

$$(18) \quad S_{\text{nematic}}^{\text{Onsager}} = -N \left[\ln \left(\rho^3 D^2 L^4 \frac{\pi}{4} \right) \right].$$

Figure 2(e) shows $S_{\text{iso}}^{\text{Onsager}}$ and $S_{\text{nematic}}^{\text{Onsager}}$ (per particle) for $L/D = 5$ and again the ordered phase has a larger entropy at large densities. As in the previous HS case, the common tangent line to the expressions S vs. V (equal P and μ) selects the densities of the two coexisting phases.

The theory of Onsager, despite its approximations, has the strong merit of highlighting the important role of orientational entropy in the ordering process of colloidal anisotropic particles. Indeed, this theory has become the starting approach for understanding more and more complex mesophases (smectic [57, 58], chiral [59], discotic [60], biaxial nematic [61], twist-bend nematic [62, 63]), progressively accompanying the synthesis of colloidal particles of more and more complex geometry [64], including ellipsoids, disks, helices and bent-shaped particles. It also provides a relevant framework for interpreting the self-assembly of colloidal particles aggregating in persistent one-dimensional structures [65-67].

2.4. Dense hard-bodies phases. – The search for the densest ordered phase in colloids interacting only via excluded volume (hard bodies) has been a central topic in soft matter in the last years. These studies, starting from oblate and prolate ellipsoids [68, 69] have now been extended to significantly more complex structures. The dense regular packing of polyhedra and non-convex particles have been thoroughly investigated numerically [70, 71] and, to a certain extent, experimentally [72]. It has been suggested that simple measures of particle shape and local order in the fluid can help predicting the final fate of their densest phases, ending either in liquid crystal, plastic crystal, or crystal states [71]. The concept of entropic bond has been proposed, based on calculation of the effective potential between particles in dense configurations. As for chemical bonds, entropic bonding can be quantified in terms of local entropy density and bond lifetimes [73, 74]. By designing the shape of the (hard) colloidal particles, these bonds can also be exploited

to control entropic valence, suggesting the possibility of exploiting these bonds to achieve the desired self-assembly. As for the nematic case discussed previously, different forms of entropy compete. For example, in the case of regular polyhedra, rotating the particle with respect to its symmetry axis produces the same local geometry, stabilising in some cases rotational phases. It has also been suggested that shape and mixing entropy can be exploited to favour required crystal structures in mixtures of hard bodies of different shape [75].

Very recently, Glotzer and coworkers [76] reported a quite intriguing and novel phenomenon. Investigating a one-component system composed of hard particles with specific shapes, the authors discover the presence of a fluid-fluid transition which precedes crystallization. While it is known that hard particles can have several mesophases (the nematic phase is just one of them), these mesophases are usually characterized by some partial ordering process (orientations in the case of nematic phases). As we have seen, an intermediate phase is also observed in hard disks. Lee *et al.* [76] showed that for three different particle shapes, designed to favour clustering into one-, two- and three-dimensional clusters, the fluid first transforms into a higher-density fluid via a first-order fluid-fluid transition and then crystallizes. But both the low- and the high-density fluid are disordered over macroscopic scales, both in position and orientation. Order manifests itself at shorter ranges, via the formation of specific geometry-related motifs. Also the resulting crystal phases are quite interesting, being characterized by very large unit cells. This study provides a beautiful example of how relevant entropy can be in controlling self-assembly of colloidal particles.

3. – Entropy in the ground state

3.1. Patchy colloids: sampling the ground state. – Colloidal particles with novel shape and surface patterning are constantly synthesised in laboratories all over the world [3, 4, 29, 12, 6, 7, 14]. These novel nano- and micron-sized particles hold promise to become the building blocks of tomorrow tunable materials, significantly expanding over atomic and molecular compounds. An interesting class of these novel colloidal particles is constituted by limited-valence colloids, particles with ability to selectively bind to a controlled number of neighbors [77] providing specificity to the particle-particle interaction. This binding specificity is achieved by particles design, as in DNA nano-stars [16], or via specific patterning of the surface properties which can be decorated by well-defined patches (for example hydrophobic or hydrophilic areas [11]) or functionalised with specific molecules (including DNA single strands [78]). These directional colloids, besides providing the community with the nano- and micro-size analog of molecules, significantly expand the possibilities offered by quantum mechanics in the design of the inter-particle interactions.

When the valence is limited, on cooling the particles start to cluster forming larger and larger aggregates, eventually giving rise to a network in which the nodes are the particles and the functionality of the network (the number of links departing from each node) is provided by the particle valence. Differently from supramolecular chemistry systems [35], colloidal bonds are not permanent. The ability to break and reform bonds makes it possible for the system to avoid any trapping in a metastable state and, at low T , to reach a condition in which all possible bonds are formed, *i.e.* to sample the ground state.

3.2. Liquid or crystal again: the role of bond flexibility. – The ability of limited-valence patchy colloidal particles to form a fully bonded network adds an interesting twist in the low-temperature behavior of these systems. As stated in textbooks, all substances (except helium, owing to quantum effects) crystallize at low T . The lower energy of the ordered phase compared to the disordered one, together with the vanishing role of entropy on cooling (entering in the free energy with a multiplicative T factor) explains the inevitable crystallization ability of all atomic and molecular systems. But this explanation ceases to be applicable when the disordered liquid has the same energy as the ordered crystal, as it is the case in these novel colloidal particles. As for the HS colloid case, entropy becomes the main factor ruling the relative thermodynamic stability of the liquid and of the crystal, opening the unexpected possibility that, for a suitable choice of the inter-particle interaction, the disordered state can remain the thermodynamically stable phase down to vanishing T .

A recent study [79] has demonstrated that it is possible indeed to design patchy colloidal particles which never crystallize in a wide range of densities, being the disordered network the lowest free energy state at all T . To grasp why this is possible, we have to focus on the entropy of the liquid and of the crystal. As for the HS case, both phases have vibrational entropy, originating both from the constrained center-of-mass motion and from the molecular rotations, a measure of all microstates which can be sampled by the system at fixed bonding pattern. In these network-forming fluids, the bonds provide energetic cages which constrain the motion of the particles [80], similarly to the excluded-volume cage confining particles in glasses. As for the HS case, the ordered configuration has a larger vibration entropy. As we have discussed in the HS section, crystal cages are more regular, allowing on average a larger mean square displacement of the particles. Again, as for the HS case, the disordered phase has an additional entropic stabilisation arising from the different disordered arrangement of all particles compatible with a fully bonded network. The freedom to modify the parameters of the interaction potential, a possibility missing in the HS case, makes it possible to tune the configurational entropy of the liquid. In particular, it has been shown that the flexibility of the bonds (encoded in the angular patch width) has a strong effect on the strength of the liquid configurational entropy. The patch width, a quantity which can be controlled in the design of patchy colloidal particles, then becomes a key element in controlling the entropy of the liquid as compared with that of the crystal.

As shown in ref. [79], on decreasing the directionality of the bonds the liquid entropy progressively increases, becoming larger than the crystal entropy for rather flexible bonds. The increase in the number of distinct fully bonded networks arises from the possibility, offered by very flexible bonds to increase the diversity of the close-bond rings. For very flexible bonds the network topology includes closed rings formed by three and four consecutive links (fig. 3(a)). This significantly increases the configurational part of the network entropy compared to the diamond crystal topology in which only rings of six are present. The larger liquid entropy, in the density region where the fully bonded network can form, stabilizes the liquid phase which becomes, beyond a certain threshold angle, the stable phase even at very low temperatures (fig. 3(d)). Figure 3(e) and (f) compare the phase diagram of two tetrahedral patchy models (with valence four), differing only in the patch width. In the case of quite directional bonds, the standard scenario is observed. The stability field of the open diamond crystal structure meets with the gas-liquid coexistence curve at the triple point, such that the low T phases are the gas phase and the crystal phases. When bonds become more flexible, the diamond crystal loses its thermodynamic stability and a funnel of liquid states opens up at intermediate densities

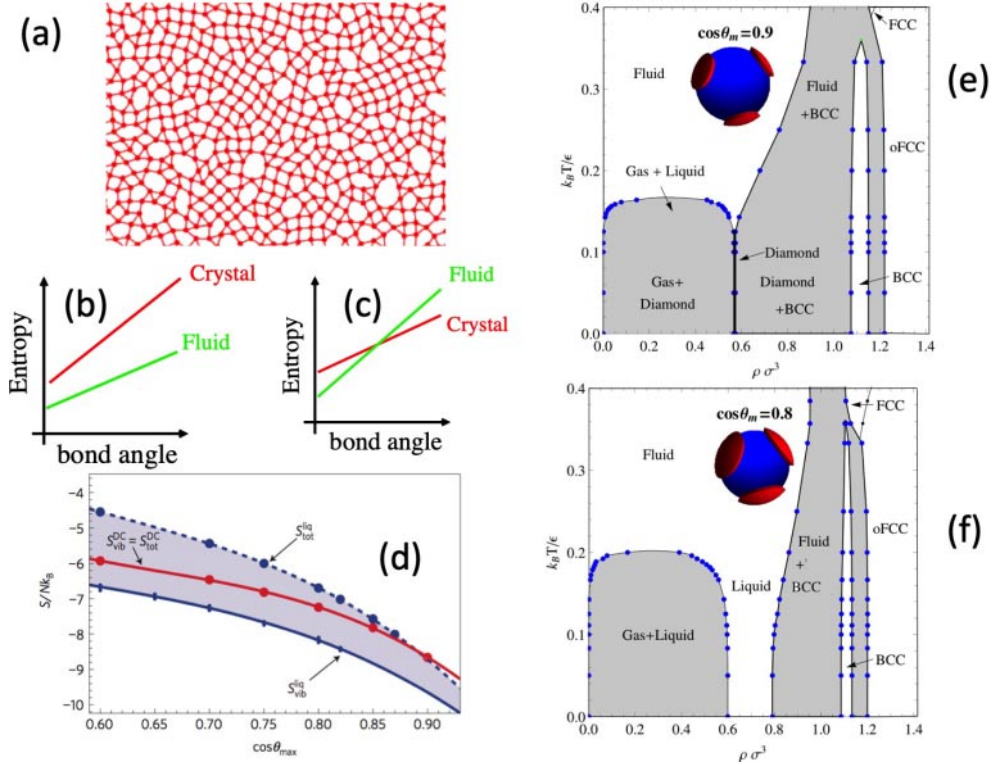


Fig. 3. – Effect of the bond flexibility on the phase diagram of tetrafunctional patchy particles. (a) A cartoon of a two-dimensional network of fully bonded particles connected by flexible bonds, highlighting the diversity of bond topologies. Closed rings of bonds of different size (starting from three) are shown. (b-c) Schematic plot of two possible behaviors of the crystal and fluid entropy (both fully bonded) with the flexibility, as encoded in the patch width. (b) The case corresponding to a crystal which is always more stable than the fluid (larger entropy). (c) The case in which, beyond a cross-over patch width, the fluid entropy becomes larger than the crystal one. (d) Estimate [79] of the liquid and diamond crystal (DC) entropies as a function of the width of the patch. The liquid entropy is separated in its two component: vibrations at fixed bonding pattern and configurational (counting the number of different networks topologies compatible with the fully bonded state). The crossing point between the total liquid entropy and the DC entropy indicates the patch width value beyond which the fully bonded liquid is the thermodynamically stable phase. Calculated phase diagrams [79] for a directional (e) and a flexible (f) case. In the latter case, a funnel of thermodynamically stable liquid states extending to vanishing temperatures is found between the gas-liquid phase coexistence and the region of stability of the dense crystals (body-centered cubic BCC and face-centered cubic FCC). ((d-f) redrawn from ref. [79]).

between the gas-liquid and the liquid dense-crystal coexistence regions. In this density funnel, the disordered fully bonded network remains the stable state down to vanishing T .

The idea that bond flexibility, by increasing the entropy, favours the thermodynamic stability of disordered fully bonded systems is not limited to patchy colloids in three dimensions, but has found important application in the interpretation of the phase behavior of several two-dimensional systems [81].

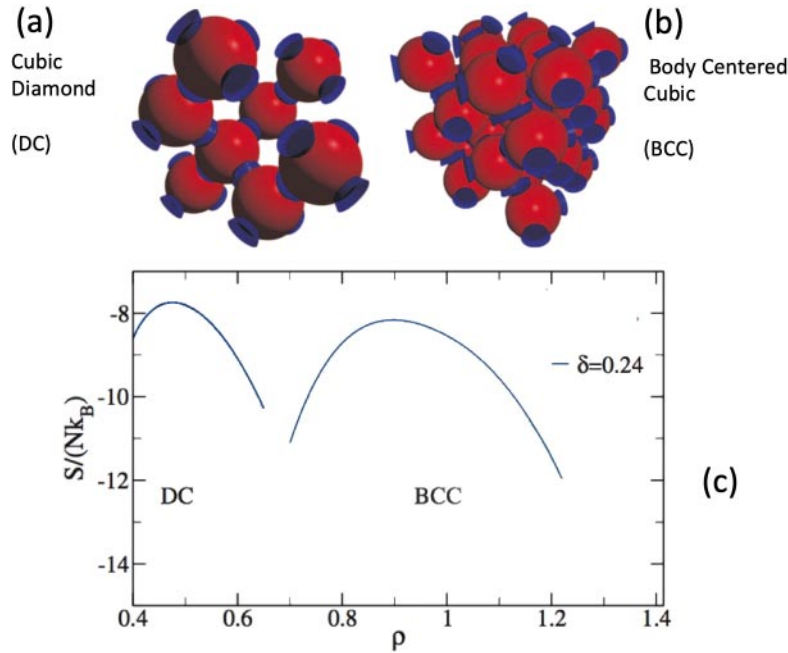


Fig. 4. – Cartoons of the (a) Cubic Diamond (DC) structure formed by tetrafunctional patchy colloidal particles and of the (b) Body Centered Cubic (BCC) structure. (c) The entropy of the two crystals as a function of density (redrawn from ref. [88]) for a Kern-Frenkel model with interaction range 0.24σ .

The discovery that limited-valence models with flexible bonds can give rise to thermodynamically stable phases is also of relevance to the physics of glasses. They indeed provide a neat example of systems which can slow down their dynamics on cooling without ever crystallizing. In this respect, they constitute models for an ideal glass, a system which never crystallizes and for which the ground state can be reached in thermodynamic equilibrium (at least in finite-size systems). Systems composed of limited-valence particle retain configurational entropy even at vanishing temperatures [82, 83, 79]. The dynamics in flexible patchy systems, the flexible analogues of the atomic and molecular network glass formers [84], both on the computer and in the real world [85] follow an Arrhenius dynamics with an activation energy related to the bond strength. In these systems, the Kauzmann temperature [86] is zero.

3.3. Entropy selection of the stable crystals. – As discussed previously, particles decorated by a limited number of patches, with interactions which can be assumed to be quantized (on-off bonds), possesses a well-defined ground state, defined by the condition that all possible bonds are formed. When this condition is met, the role of entropy as the only driving force for selecting the thermodynamically most stable phase among all possible fully bonded structures is re-established. Entropy does not only control the relative stability of the fully bonded disordered network compared to the ordered crystals, but also the relative thermodynamic stability of the different ordered fully bonded polymorphs.

Tetrahedral patchy particles offer a good example of this entropy selection. Indeed, besides the diamond crystal, it is also possible to form denser lattices in which particles

retains their tetrahedral coordination. Examples of these lattices are the sodium-thallium crystal (NaTl, consisting of two interpenetrating diamond crystals), the body-centred-cubic (bcc) crystal and the fascinating open clathrate structures, in which fully bonded tetrahedral particles arrange into crystalline cages of different diameter [87]. It has been found that at ambient pressure the less dense diamond lattice is the thermodynamically stable phase [88]. Figure 4 shows the density dependence of the entropy evaluated via thermodynamic integration from the Einstein model [89,90] for the DC and two interpenetrating DC lattices. Similarly to what we have seen for the case of hard spheres and hard cylinders, a common tangent construction allows us to calculate the coexistence between the two crystals and their region of thermodynamic stability.

A similar role of the vibrational entropy in stabilising open crystals has also been recently predicted [91] for mobile DNA-coated colloids [92,93]. These colloidal particles are covered by a layer of mobile DNA strands, which can be recruited in the presence of a nearby particle coated with complementary DNA effectively forming patches on demand. Interestingly, the amount of DNA coated on the particle surface controls the number of patches that each colloidal particle can form [94,95]. Despite the valence selection mechanism is not yet fully clarified, even in this type of colloidal particles at low T fully bonded conditions are achieved, leaving entropy as main driving force for crystal selection.

Another case in which the orientational contribution plays an important role in the crystal selection is offered by triblock Janus particles [11], colloidal particles decorated with two hydrophobic poles of a tunable area separated by an electrically charged middle band. Upon addition of salt, the overall electrostatic repulsion is screened and the hydrophobic patch-patch interaction becomes the dominant interparticle interaction. The patch width in the experimental system, of the order of 65 degrees, allows the simultaneous bonding of two particles per patch for geometric reasons (a minimum angle of $\pi/3$ is requested to realize a two-bonds-per-patch condition). Under high-salt conditions, particles form all possible bonds by creating a four-coordinated structure known as a Kagome lattice [11] (fig. 5(a) and (e)). These particles provide a good example of design-controlled self-assembly, since by selecting the patch width it is possible to control the maximum number of bonded neighbours [96]. The equilibrium phase diagram, calculated in ref. [97], predicts, besides a fluid phase, a coexistence of the Kagome lattice with a triangular phase (fig. 5(a)).

As for the tetrahedral patchy particles, also for the triblock Janus particles translational entropy favours the open crystal lattices [98]. In the open crystal, particles have indeed larger vibrational amplitudes. Interestingly, in the case of triblock Janus particles the Kagome lattice is not the only possible open crystal (fig. 5(f,g)). Here, orientational entropy [98] plays the dominant role in selecting the Kagome as the thermodynamic most stable structure. In two dimensions, orientational entropy is a measure of the angle that a particle can explore without breaking the hydrophobic bond. The Kagome lattice is indeed the one (see fig. 5(c,e)) for which the rotational angle is largest.

3.4. Vitrimers: entropy-driven dynamics in the ground state. – Very recently, an innovative class of polymeric reconfigurable covalent networks, named vitrimers (fig. 6(a)), has been synthesized [99]. The name originates from their dynamical properties, which fall into the category of strong glass formers [102]. Just like silica glass, these materials can be heated and reworked to take any shape without dissolving. The evolution of the network topology is controlled by a properly designed bond swap mechanism (controlled via a thermally sensitive catalyst) that preserves the total number of bonds. The

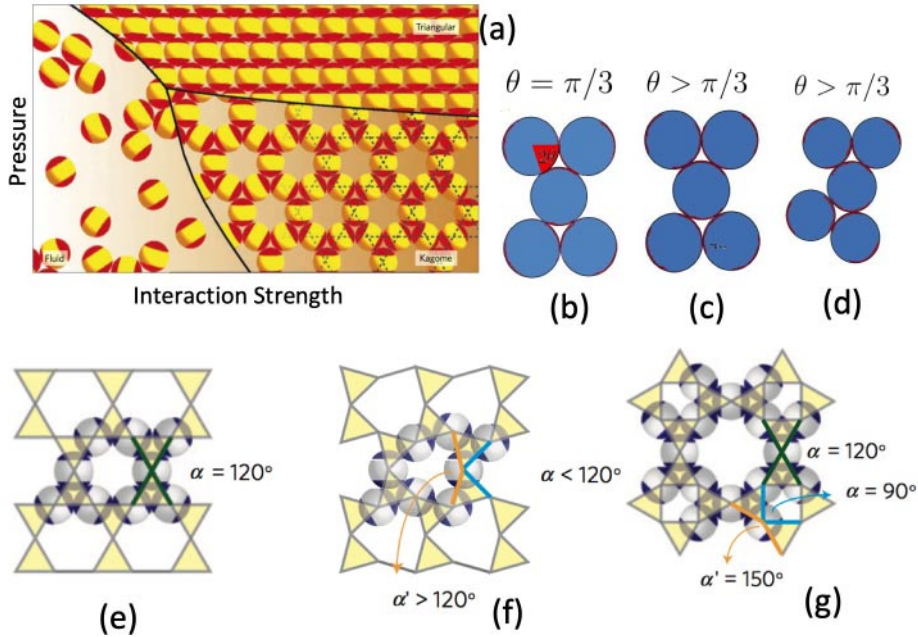


Fig. 5. – Triblock Janus particles in two dimensions. (a) The calculated equilibrium phase diagram showing the isotropic liquid phase, the Kagome lattice at small pressure and high interaction strength and the dense triangular lattice at high pressure (redrawn from ref. [97]). In both crystals the energy is the same since the patch width allows at most two bonds per patch. A bond is present if the line connecting the particle centers passes by both patches. (b-d) Cartoon of the possible orientation of a central particle surrounded by four other bonded ones. In (b) the patch width is exactly $\pi/3$ and the central particles can not rotate without breaking a bond. In (c) the patch width 2θ is larger than $\pi/3$ showing that the central particle can rotate by an angle equal to $2\theta - \pi/3$, providing rotational entropy to this lattice. In (d) the same patch width is shown, but for particles arranged in a less symmetric lattice. This reduced symmetry reduces also the amplitude of the possible rotations of the central particle. Cartoon of the Kagome lattice (e) and of two other open but less symmetric fully bonded lattices (f-g), which are topologically possible but entropically less favoured than the Kagome lattice (redrawn from ref. [98]).

bonds provide rigidity typical of plastics but the reconfiguration makes it possible to relax internal stress and to drive the system toward its minimum free energy state. The physics of vitrimers builds on polyfunctional condensation [35] of binary mixtures when only bonds between monomers of different type are possible. When N_A A -particles with functionality f_A are mixed with N_B B -particles with functionality f_B , the relative concentration in the system $x = N_A/(N_A + N_B)$ controls the low- T state. In stoichiometric conditions ($N_A f_A = N_B f_B$) when all possible bonds are formed the resulting network is fully bonded and no free links exist. When off-stoichiometric compositions are selected, the minority species forms all possible bonds, while the majority species remains with some of its binding sites unsatisfied [103]. The unbonded binding sites are thus available, if a swap mechanism is present, to substitute sites involved in existing bonds, allowing for network reconfiguration. Since the total number of bonds (the energy) is always constant, ideally the evolution of the system is only controlled by the maximisation of entropy [100].

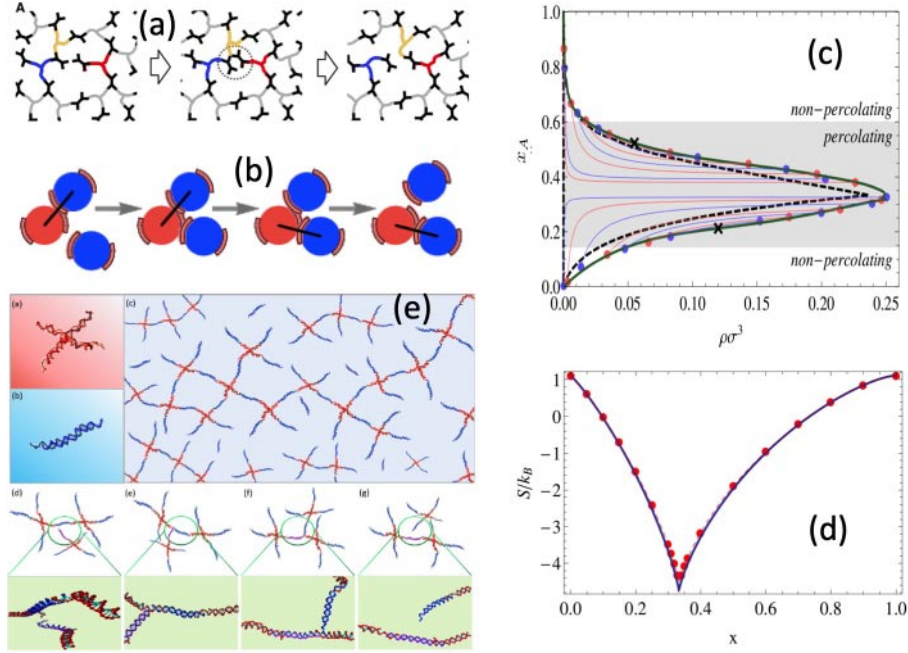


Fig. 6. – Strolling in the bottom of the energy landscape: Vitrimers. (a) A schematic representation of the restructuring step in a polymeric network of tetrafunctional and bifunctional units. A bond swap changes the local topology without altering the total number of bonds. Redrawn from ref. [99]. (b) A patchy colloidal particle analog of vitrimers, a binary mixture of A and B patchy particles with only AB swappable bonds. (c) Theoretical and numerical phase diagram of the patchy colloidal model for the case of a mixture of valence four and valence two [100]. Thick lines are phase coexistence boundaries. Thin lines indicate the coexisting phases. The shaded area indicates the region where a spanning network (a gel) is found. (d) Comparison between the theoretical estimate of the entropy based on Wertheim theory and its numerical counterpart (redrawn from ref. [100]). (e) Cartoon of the experimentally realized [101] DNA gels in which patchy particles are made by appropriate DNA sequences. The central panel shows the swapping process. The lower panel the associated corresponding binding process (redrawn from ref. [101]).

To theoretically model vitrimers, the complexity of the particles themselves can be simplified by selecting a coarse-grained description which only preserves the fundamental ingredients: a binary mixture of A and B particles with off-stoichiometric conditions complemented by a swap mechanism (fig. 6(b)). These simple ingredients open the possibility of describing the phase behaviour of a vitrimer system (fig. 6(c)) as the $T \rightarrow 0$ case of a binary mixture of A and B patchy particles with f_A and f_B patches, respectively, with only AB interactions of strength ϵ . In this model, the number of bonds directly provides the potential energy. At low T , the number of bonds n_b is always $n_b = \min(f_A N_A, f_B N_B)$ and the energy is $U = -n_b \epsilon$.

Following Wertheim theory [104], a theory originally developed to model associating liquids and shown to provide a quite accurate description of patchy colloids [77, 105], the free energy of the fully bonded binary patchy system can be written as

$$(19) \quad F = -n_b \epsilon - T(S_{\text{bond}} + S_{\text{CS}} + S_{\text{mixing}}),$$

where S_{CS} is the reference Carnahan-Starling [41] HS entropy, S_{mixing} is the entropy associated to the mixing of the two species (A and B), and

$$(20) \quad S_{\text{bond}} = S_{\text{comb}}(f_A N_A, f_B N_B) + k_B n_b \log \frac{V_b}{V},$$

where [100]

$$(21) \quad S_{\text{comb}}(n, m) = \begin{cases} k_B \log \frac{n!}{(n-m)!}, & \text{if } n > m, \\ k_B \log \frac{m!}{(m-n)!}, & \text{otherwise,} \end{cases}$$

corresponds (assuming $m > n$) to the entropy associated with the number of ways n (distinguishable) bonds can be distributed over m patches, and is therefore associated with the configurational entropy in the system. The last term in eq. (20) represents the change in entropy from creating a bond (where V_b is the so-called bonding volume) multiplied by the number of bonds n_b . Since the total number of bonds is constant, being fixed to its largest possible value, the deciding factor entering in the free energy is entropy, rather than energy, despite the low T . The resulting entropic phase diagram is shown in fig. 6(c). At low densities a phase-separation is present. A sample prepared inside the unstable region phase-separates into a low-density phase rich of the majority component in monomeric form, and into a dense network which incorporates most of the n_b bonds. This numerical result proves that vitrimers do not dissolve when diluted. Interestingly, due to the limited valence, the theoretical estimate of the entropy represents quite well the “exact” numerical calculation (fig. 6(d)).

Very recently, an experimental realization of an all-DNA gel composed of tetra-functional DNA nanoparticles, acting as network nodes, and bi-functional ones, acting as links, capable of bond-swapping at low T , has been reported [101]. Exploiting ideas from DNA nanotechnology, the binding bases sequence incorporates an appropriate exchange reaction which allows links to swap, constantly retaining the total number of network links (fig. 6(e)). Thus, the resulting DNA gel is able to rearrange its topology at low temperature while preserving its fully bonded configuration.

4. – Entropy attracts

4.1. Depletion interactions. – One of the most powerful ways to control the attractive interaction between hard bodies is provided by the so-called depletion interaction [25]. The addition in solution of small (compared to the colloids) non-absorbing cosolutes (*i.e.* not interacting with the particles, apart from the excluded volume) induces an entropic attraction between the colloids proportional to a first approximation to the concentration of cosolutes. The physics behind this important attractive interaction was clarified by two Japanese polymer scientists, Asakura and Oosawa [23], in a study which has remained unnoticed for more than two decades before becoming a seminal contribution.

Asakura and Oosawa proposed to focus on an idealized model, *i.e.* two large hard particles of diameter σ_c (the colloids) in the presence of M small hard particles (the depletants) of diameter σ_p in a volume V (fig. 7(a-b)). They derived the statistical-mechanics description of the system to evaluate the probability to find the two colloids

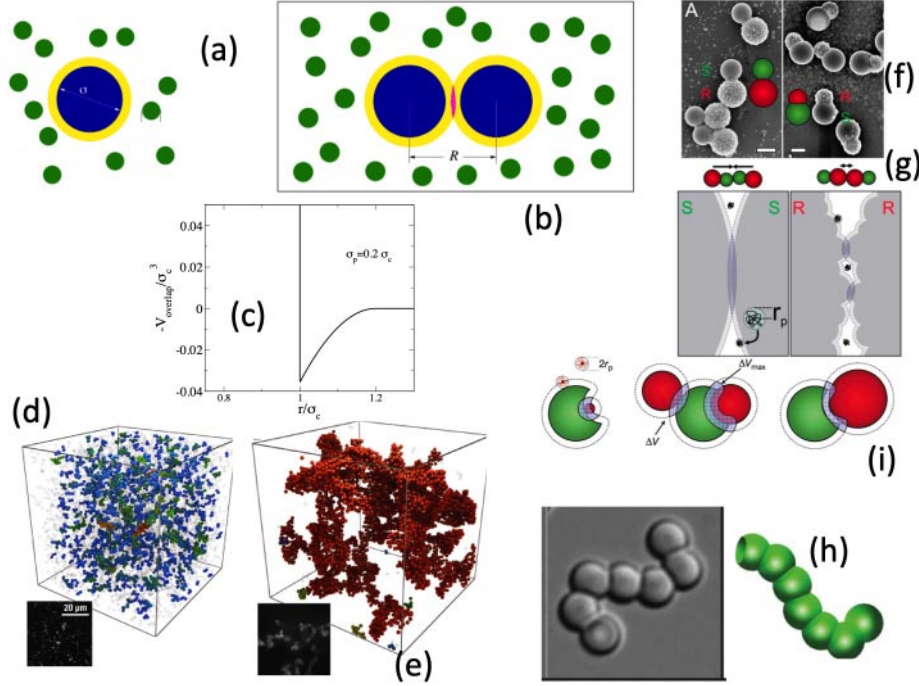


Fig. 7. – Depletion interactions: (a) A large colloidal particle immersed in a solution of small particles (usually polymers). The center of the polymer is prevented from accessing the volume occupied by the particle and the corona around it. (b) When two colloidal particles are close by, the coronas of the two particles overlap increasing the volume accessible to polymers. (c) The shape of the depletion interaction potential calculated by Asakura-Oosawa. (d-e) Confocal images of a colloid polymer mixture for two different polymer concentrations (redrawn from ref. [106]). In (d) the colloids are dispersed in a fluid phase. In (e) the depletion interaction has grown driving the system through a spinodal decomposition process, which leads to the formation of a two-phase system. In the dense phase the dynamics of the particles is strongly reduced, generating a depletion gel. (f-g) Depletion in dumbbells composed of particles with smooth and rough surfaces. The rough surface generates a smaller overlap volume and hence a less intense attraction between rough surfaces as compared to the attraction between smooth surfaces (redrawn from ref. [29]). (i-h) Lock-and-key colloids. With the appropriate size ratio of the buckled region and the colloidal particle, it is possible to maximize the excluded volume, generating a preferential binding. (h) A colloidal polymer resulting from a lock-and-key depletion mechanism ((i-h), redrawn from ref. [13]).

at relative distance r , under the simplifying assumption that the depletants do not interact among themselves (an ideal gas) but do interact via excluded volume with the two colloids.

Indicating with \vec{r} and \vec{s} the positions of the colloids and of the cosolutes, the partition function in the canonical ensemble can be written as

$$(22) \quad Q = \frac{1}{2\lambda_1^6} \frac{1}{M!\lambda_2^{3M}} \int e^{-\beta V_{11}(\vec{r}_1, \vec{r}_2)} d\vec{r}_1 d\vec{r}_2 \int d\vec{s}_1 \dots d\vec{s}_M e^{-\beta V_{12}(\vec{r}_1, \vec{r}_2, \vec{s}^M)},$$

where V_{11} is the HS potential between the colloids and V_{12} the HS potential between the depletants and the two colloids. Since V_{12} is pair-wise additive ($V_{12} = \sum_{i=1}^M v_{12}(\vec{r}_1, \vec{r}_2, \vec{s}_i)$)

$$(23) \quad Q = \frac{1}{2\lambda_1^6} \frac{1}{M!\lambda_2^{3M}} \int e^{-\beta V_{11}(\vec{r}_1, \vec{r}_2)} d\vec{r}_1 d\vec{r}_2 \left[\int d\vec{s}_1 e^{-\beta v_{12}(\vec{r}_1, \vec{r}_2, \vec{s}_1)} \right]^M.$$

The integral between square brackets is exactly the volume accessible to a single depletant, *i.e.* the total volume of the system minus the volume prohibited by the presence of the two colloids. Since the depletant-colloid distance cannot be smaller than $\frac{\sigma_c + \sigma_p}{2}$, the prohibited volume is twice V_0 , the volume of a sphere of diameter $(\sigma_c + \sigma_p)/2$ minus, if the two colloids are close by, the overlap volume V_{overlap} between the two spheres of diameter $(\sigma_c + \sigma_p)/2$. Thus,

$$(24) \quad \int d\vec{s}_1 e^{-\beta v_{12}(\vec{r}_1, \vec{r}_2, \vec{s}_1)} = V - 2V_0 + V_{\text{overlap}}(|\vec{r}_1 - \vec{r}_2|),$$

where the overlap volume can be calculated geometrically using sphere-sphere intersection properties as

$$(25) \quad V_{\text{overlap}}(r) = \frac{\pi}{12} [2(\sigma_c + \sigma_p) + r][(\sigma_c + \sigma_p) - r]^2.$$

Then

$$(26) \quad [V - 2V_0 + V_{\text{overlap}}(|\vec{r}_1 - \vec{r}_2|)]^M = (V - 2V_0)^M \left[1 + \frac{V_{\text{overlap}}(|\vec{r}_1 - \vec{r}_2|)}{V - 2V_0} \right]^M \\ \approx (V - 2V_0)^M \left[1 + M \frac{V_{\text{overlap}}(|\vec{r}_1 - \vec{r}_2|)}{V - 2V_0} \right] = (V - 2V_0)^M [1 + \rho_M V_{\text{overlap}}(|\vec{r}_1 - \vec{r}_2|)],$$

where $M/(V - 2V_0) \equiv \rho_M$ is the number density of small spheres. Inserting this result in eq. (23), it is apparent that the two large colloids interact with a total interaction potential which is the sum of the original HS (V_{11}) potential complemented by an effective potential $V_{\text{eff}}(r)$ induced by the presence of the cosolutes whose r dependence is (fig. 7(c))

$$(27) \quad V_{\text{eff}}(r) = -k_B T \ln[1 + \rho_M V_{\text{overlap}}(r)] \approx k_B T \rho_M V_{\text{overlap}}(r) = \Pi V_{\text{overlap}}(r),$$

where $\Pi \equiv k_B T \rho_M$ is the ideal gas pressure originating from the cosolutes.

We note on passing that an alternative but equivalent derivation can be formulated in terms of the net force induced by the osmotic pressure on the surface of the two colloids. While when the two large particles are far apart the cosolutes hit the colloids symmetrically, when the two large particles are close-by, the cosolutes are excluded in the overlap volume region, producing a net unbalance in the average pressure which pushes inward the two colloids. The analytic derivation of the unbalanced pressure, which can be found in ref. [25], provides the same expression for the effective potential as the one in eq. (27). Thus, the essence of the depletion interaction is the tiny gain of entropy experienced by each cosolute when colloids are close by (and V_{overlap} is different from zero), originating from the possibility of additionally exploring the overlap volume. This entropy gain, once multiplied by the large number M of small cosolutes, results into a

net attractive potential between the two colloids, which can easily become of the order of the thermal energy $k_B T$. The concentration of cosolutes then determines the strength of the interaction while their size determines the interaction range, explaining the large versatility of depletion interaction in the design of effective potentials between colloids.

Depletion forces have found several applications in colloidal science to induce crystallization [26], phase separation [107], shape fractionation [28]. The ability to control the interaction range has been exploited to investigate the existence of the liquid state [108], colloidal gelation [106] (fig. 7(d-e)), glass-glass transitions [109,110]. More recently, depletion interactions have been exploited to control the self-assembly of dumbbells composed of fused spheres of different surface roughness [29,111] (fig. 7(f-g)) and of colloidal particles with indented surfaces [13] (fig. 7(h-i)), to imitate the lock-and-key mechanism of protein selectivity. The different overlap volume between rough and smooth spheres and between locks and keys of comparable size is the crucial element in the self-assembly process. The same physics can also be exploited to direct the motion of colloidal particles on properly patterned surfaces [27] or to drive crystallization on patterned surfaces [112]. Recently, depletion interactions arising from highly polydisperse cosolutes clusters, typical of systems in proximity of a sol-gel transition, have been evaluated numerically [31]. The observed exponential attractive effective potential and the tunable range of the interaction (depending on the distance from percolation) suggests a similarity with critical Casimir forces [113,30].

4.2. Entropic effective potential: from two dimensions to quasi-two dimensions. – Another interesting case where entropy displays its power in defining the effective potential between colloidal particles is offered by HS in strong confinement, a topic which has recently received renewed interest [114,115]. If HS are constrained in a slab of width σ , the system clearly behaves as a two-dimensional hard-disk system (of diameter σ), which, as we have discussed previously, is characterized by a hexatic mesophase between the isotropic and the crystal ones.

If the slab confinement is slightly larger than σ , *i.e.* $\sigma + L$, with $L \ll \sigma$, the center of the hard spheres can explore a perpendicular section of length L . This additional freedom (entropy) transforms the hard-disk interaction potential in a novel effective 2D potential, composed of a renormalized hard-disk potential of diameter $\sqrt{\sigma^2 - L^2} < \sigma$ decorated by an additional soft repulsion. Calling \hat{z} the direction normal to the plane, x and y the coordinates along the plane and $t = \sqrt{x^2 + y^2}$ the radial distance projected on the xy plane, the effective potential $\beta V_{\text{eff}}(t)$ in the two-body approximation can be calculated by evaluating the configurational part of the partition function for two hard spheres in a slab, one of the two fixed at the origin of the plane ($x_1 = 0, y_1 = 0$) and free to move only in the z -direction (see fig. 8). The second particle is located at radial distance $t = \sqrt{x_2^2 + y_2^2}$, exploring all possible z_2 values. The partition function can be written, considering for symmetry only negative values of z_1 (and adding the factor of 2 in front of the integral to compensate)

$$(28) \quad Z(t) = \begin{cases} 0, & t < \sqrt{\sigma^2 - L^2}, \\ \frac{2}{L^2} \int_{-L/2}^0 dz_1 \left\{ \int_{z_1 + \sqrt{\sigma^2 - t^2}}^{L/2} dz_2 + \int_{-L/2}^{z_1 - \sqrt{\sigma^2 - t^2}} dz_2 \right\}, & \sqrt{\sigma^2 - L^2} < t < \sigma, \\ 1, & t > \sigma. \end{cases}$$

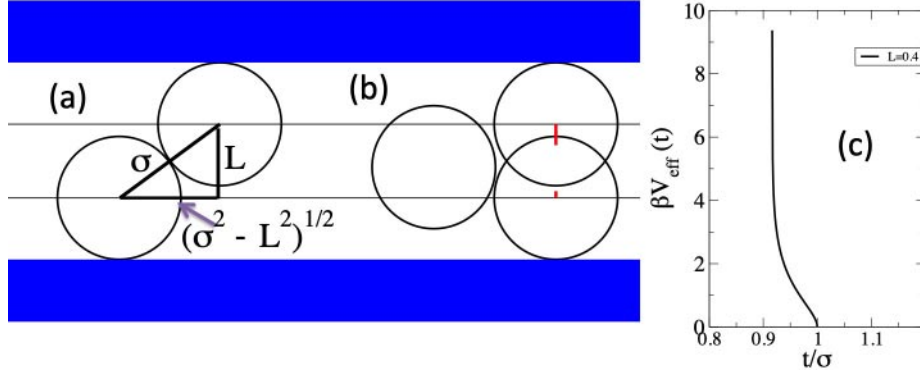


Fig. 8. – Cartoon of hard spheres in a slab of width $L + \sigma$. The centers of the spheres are confined in the z -direction in a slab of width L . (a) In the limit of $L \ll \sigma$, the distance of closest approach projected on the xy plane is $\sqrt{\sigma^2 - L^2}$. The red lines in (b) indicate the possible values of z_2 (corresponding to the two integration intervals in eq. (28)), for a fixed z_1 value. (c) Resulting 2d effective potential (eq. (30)) formed by a hard-disk component of diameter $\sqrt{\sigma^2 - L^2}$ followed by a soft entropic interaction potential arising from the possibility of exploring different z_1 and z_2 values at fixed t , for $L/\sigma = 0.4$.

In the region of interest, $\sqrt{\sigma^2 - L^2} < t < \sigma$, the solution of the two integrals gives

$$(29) \quad Z(t) = \frac{2}{L^2} \frac{(L - \sqrt{\sigma^2 - t^2})^2}{2},$$

corresponding to

$$\beta V_{\text{eff}}(t) = \begin{cases} \infty, & t < \sqrt{\sigma^2 - L^2}, \\ -\ln Z(t) = -2 \ln \left(1 - \sqrt{\frac{\sigma^2 - t^2}{L}} \right), & \sqrt{\sigma^2 - L^2} < t < \sigma, \\ 0, & t > \sigma, \end{cases}$$

describing a hard-disk potential (with diameter $\sqrt{\sigma^2 - L^2}$, smaller than σ) followed by a potential which diverges logarithmically for $t \rightarrow \sqrt{\sigma^2 - L^2}$ and reaches zero as a square root for $t \rightarrow \sigma$.

This interesting example shows how the transition from a pure 2D system to a quasi-2D system takes place and how the additional entropy generated by the availability to sample the direction orthogonal to the plane affects the effective potential in the limit of extreme confinement. Franosh and coworkers [114] have shown that the pure 2D phase transitions are robust and survive small non-vanishing L . The disappearance of the hexatic phase under addition of disorder in the particle diameters [56] correlates with the disappearance of the hexatic phase on moving from 2D to quasi-2D [115].

4.3. Combinatorial entropy: microemulsion droplets linked by telechelic polymers. – Another source of entropy, different from the translational, orientational, or depletion cases we have previously discussed, plays an important role in soft matter self-assembly processes. This entropy arises from the different combinatorial ways one can distribute

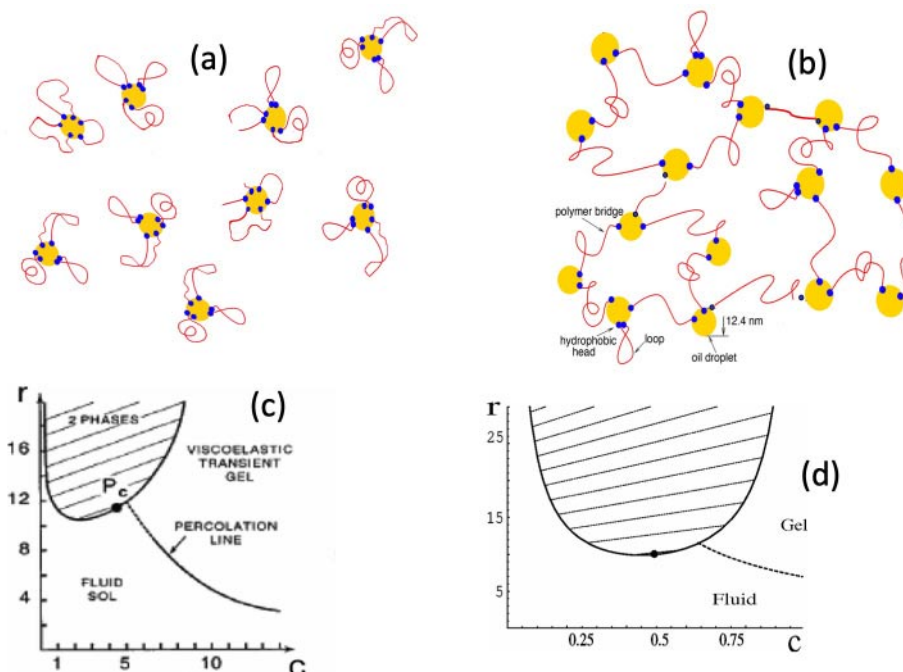


Fig. 9. – Cartoon of the microemulsion droplets (yellow spheres) connected by telechelic polymers (red) with hydrophobic ends (blue). (a) A schematic representation of a gas-like phase in which both ends of the polymers are immersed in the same droplet. (b) A dense percolating liquid-like phase, in which polymers connect different droplets. (c) Experimental phase diagram showing a phase coexistence between a dilute and a dense phase of droplets, induced by the increase in the number of polymers per droplet r (redrawn from ref. [116]). (d) Theoretical phase diagram (redrawn from ref. [32]).

bonds between distinct clusters. One interesting case is offered by a solution of microemulsion droplets linked by telechelic polymers [116]. The two hydrophobic ends of each polymer are energetically constrained to reside inside the oil droplets, in the same or in two different ones. Thus, the polymers can provide links between different droplets. To a first approximation, energy does not play a relevant role and the behaviour of the system is mainly controlled by the different ways the polymer ends can be distributed over the accessible droplets.

Ideally, since all ends must be inside oil droplets, one would think that the state of maximum entropy is the one in which both ends of the polymers reside in the same droplet (fig. 9(a)). Indeed, in this configuration all droplets retain their translational freedom. Binding between droplets to generate a connected structure (fig. 9(b)) would imply a loss of translational entropy. This simple argument neglects the fact that the possibility to connect with neighbouring droplets significantly increases the number of microstates so much to overcome, beyond a certain packing fraction and beyond a certain number of polymers per droplet, the loss of translational entropy upon binding.

A theoretical analysis of this system, highlighting the importance of the combinatorial entropy has been presented in ref. [32]. The authors propose to write a zero-order free energy as a function of two independent parameters: the droplet concentration $\rho_d = \frac{N}{V}$

and the polymer concentration $\rho_p = \frac{N_p}{V}$. By neglecting coupling between the droplets and the polymers, the free energy can be expressed as $\beta F = \beta F_{\text{droplet}} + \beta F_{\text{polymer}}$, where

$$(30) \quad \beta F_{\text{polymer}} = -N_p \ln Z_p, \quad \text{with } Z_p = N \frac{\Sigma_d}{\Sigma_p} \left(\frac{\Sigma_d}{\Sigma_p} + N_d^{\text{accessible}} \frac{\Sigma_d}{\Sigma_p} \right).$$

Here $N_d^{\text{accessible}} \sim \rho_d$ indicates the number of droplets that can be connected by a polymer originating in an arbitrary selected droplet. Note that we have assumed that $\frac{\Sigma_d}{\Sigma_p}$ is the number of attachment points on a droplet (proportional to the surface area Σ_d of the droplet divided by the surface area Σ_p of the polymer head). Each polymer can then end on the same droplet with probability $\frac{\Sigma_d}{\Sigma_p}$ and on a distinct but accessible droplet with probability $N_d^{\text{accessible}} \frac{\Sigma_d}{\Sigma_p}$. Note that the polymer free energy does not incorporate any energetic contribution.

The system is thermodynamically stable if the free energy is a convex function of both ρ_p and ρ_d . This means that the second derivative of the free energy ($\delta^2 F = F_{\rho_d, \rho_d} \delta \rho_d^2 + 2F_{\rho_d, \rho_p} \delta \rho_d \delta \rho_p + F_{\rho_p, \rho_p} \delta \rho_p^2$) has to be positive. Equivalently, the matrix

$$(31) \quad \begin{pmatrix} F_{\rho_d, \rho_d} & F_{\rho_d, \rho_p} \\ F_{\rho_d, \rho_p} & F_{\rho_p, \rho_p} \end{pmatrix}$$

must possess two positive eigenvalues, allowing us to separate stable from unstable states (mean-field spinodals). The results of the calculations for different values of the number of polymers per droplet r are shown in fig. 9(d) and compared with the corresponding experimental data (fig. 9(c)). Beyond a critical value of r , at low densities the system prefers to phase separate in a gas phase of droplets, in which polymers start and end in the same droplet, and in a connected phase (a network) in which the ends of the polymer preferentially explore the interior of different droplets. The connected phase emerging from the entropic phase separation constitutes a dense gel phase, being the number of connections per droplet significantly larger than the percolation threshold.

4.4. Combinatorial entropy: DNA grafted particles. – Another interesting and very recent application, where combinatorial entropy plays an important role in controlling attraction between particles, is found in DNA grafted colloids. These are gold (at the nanoscale) or polymeric particles coated with DNA strands [117-119]. The DNA strands end with a specific sequence \mathcal{A} (sticky end) that can bind to complementary sequences $\bar{\mathcal{A}}$ on nearby coated colloids.

If the particles are grafted with both \mathcal{A} and $\bar{\mathcal{A}}$ sticky ends [120, 121] (or if \mathcal{A} is self-complementary and, thus, able to bind to itself satisfying the Watson-Crick pairing rules) the situation is analogous to the microemulsion droplets linked by telechelic polymers [116]. Indeed particles can always satisfy their bonds (exploiting intra- or inter-particle links), rendering the energetic contribution to binding irrelevant [122]. In this case, again, only the combinatorial contributions dictate the net attraction between the particles. This is quite relevant since, for several-bases-long sticky sequences, the binding energy can easily become dozens of $k_B T$ which would suggest at a first glance an irreversible aggregation process. Differently, the combinatorial term can be tuned to be of the order of a few $k_B T$, making a reversible self-assembly process possible, especially if the bonding scheme is associated to a toehold displacement mechanism [123].

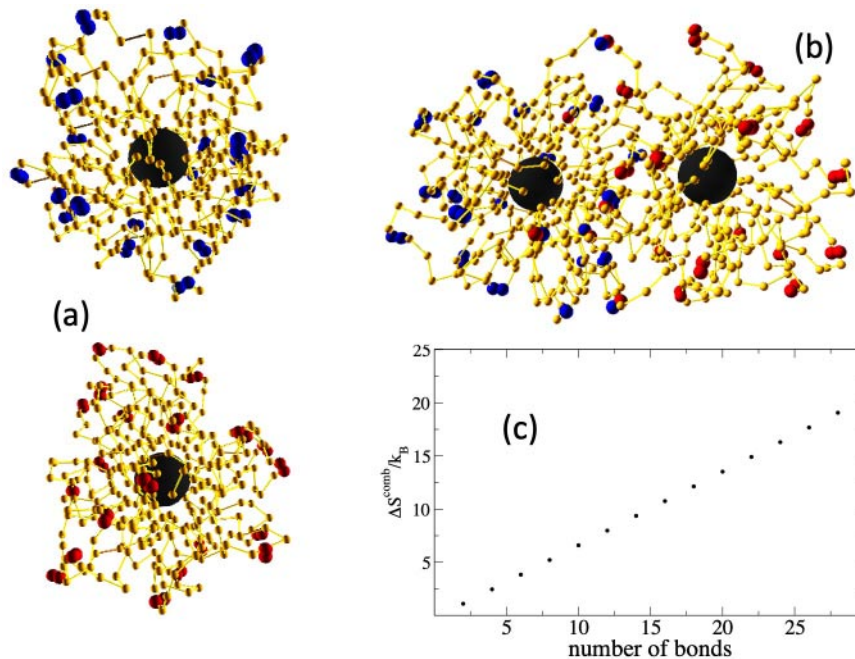


Fig. 10. – Cartoon of a nanoparticle (black) decorated by grafted polymers ending with a sticky sequence (blue and red, respectively). (a) Two isolated particles in which all sticky ends form intraparticle bonds. (b) Two close-by particles in which some of the bonds involve chains of different particles (red-blue pairs). (c) Combinatorial entropy change associated to the formation of interparticle bonds. Redrawn from ref. [122].

To clarify the role of combinatorial entropy in the case of palindromic DNA sticky sequences $\mathcal{A} = \bar{\mathcal{A}}$, consider the case of two particles with grafted polymers ending with a sticky site that can bind to only one other distinct sticky site (see fig. 10). When the particles are far, all sticky sites find their own partner among chains grafted on the same particle. At low T , all sticky sites are essentially paired. One would then expect that under these conditions there is no additional energetic gain that can compensate for the loss of translational entropy upon inter-particle binding. Instead, when the particles probe distances x compatible with intra-particle binding (see fig. 10) a finite number $B(x)$ of chains on each particle can bind to partners grafted on the other particle.

To estimate the strength of the entropic attraction, let us focus on this pool of approximately $2B(x)$ interacting sites, which can pair to form $B(x)$ bonds. If each site can bind to any other site, independently of where the corresponding chain is grafted, then the number of distinct bonding patterns is $(2B(x) - 1)!!$ (being $!!$ the symbol for double factorial). Indeed the first site can bind to $2B(x) - 1$ other sites, the first of the remaining $2B(x) - 2$ sites can bind to $2B(x) - 3$ others, and so on, resulting in the double factorial term. If instead a site can only bind to sites of the same particle, then the number of distinct bonding configurations is $(B(x) - 1)!!$ for each particle. Thus, the change in entropy introduced from allowing inter-particle binding can be quantified as

$$(32) \quad \frac{\Delta S^{\text{comb}}(x)}{k_B} = \ln \left[\frac{(2B(x) - 1)!!}{[(B(x) - 1)!!]^2} \right].$$

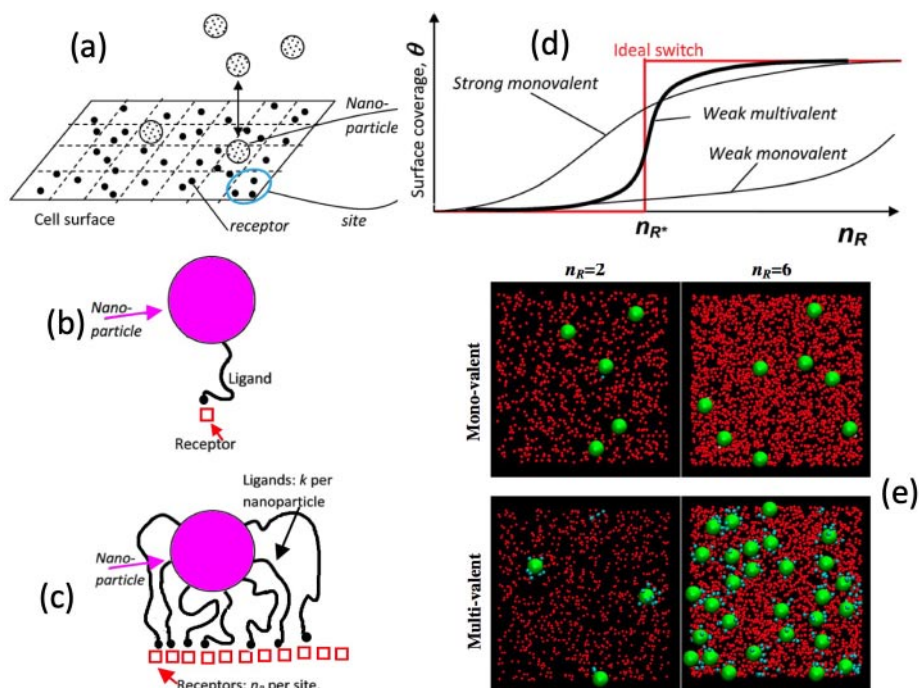


Fig. 11. – Superselectivity: (a) A schematic representation of a surface covered with receptors and exposed to a solution containing nanoparticles decorated with ligands. (b) The case of a single ligand per nanoparticle. (c) The case of multiple ligands. (d) Comparison between the adsorption efficiency of mono- and multivalent nanoparticles, contrasted with the ideal case of an on-off behavior. (e) Simulation results modelling the different adsorption properties of monovalent and multivalent nanoparticles. In both cases, the concentration of the receptors is increased by the same amount from left to right. In the case of the multivalent particles, the increase in the concentration of receptors significantly increases the number of colloidal particles adsorbed on the surface. ((a,d,e) redrawn from ref. [124]).

For typical nanoparticles grafting densities, $B(x) \sim 5\text{--}25$, corresponding to entropic attraction $\Delta S^{\text{comb}}/k_B \sim 2.7\text{--}16$. Such entropic contribution is sufficient to compensate the repulsive contribution arising from the overlap between the brushes, and to provide a net attractive potential sufficiently strong to drive aggregation of the colloidal particles into a dense liquid or into a crystal phase.

4.5. *Combinatorial entropy: superselectivity.* – As a last example of the importance of combinatorial entropy, let us focus on the binding between a ligand and a receptor (fig. 11(a)), a topic of high relevance in biological physics as well as in materials mimicking biological functions. Usually the association between two distinct particles, either macromolecules, proteins, or colloids, is controlled by the balance between the strength of interaction and the number of microstates associated to the bonded state. The resulting association efficiency (*i.e.* the probability of finding the two particles bonded) increases on cooling and/or increasing the concentration, typically following a sigmoidal curve. To increase the on-off efficiency of the binding process requires some cooperative enhancement of the binding process. In a recent study [124], the power of combinatorial

entropy has been exploited to design a super-selective binding particle. Based on the idea that the binding strength can be enhanced if there are many possible equivalent binding sites among receptors and ligands [125], the authors of ref. [124] proposed to decorate the particle with a multiplicity k of ligands, each of them weakly interacting with one of the n_R receptors (fig. 11(c)). The bonded state now can be realised with a much larger number of microstates, differing in the number of bonds $\#_b$, which can vary between one and $\min(k, n_R)$. In addition, for each number of receptor-ligand bonds $\Omega(\#_b)$, the total number of microstates is the product between the number of ways $\#_b$ elements can be selected out of k [$k(k-1)(k-2)\dots(k-\#_b)$]—normalised by $k!$ to account for the indistinguishability of the ligands—times the number of ways $\#_b$ bonds can be distributed over n_R sites ($[n_R(n_R-1)(n_R-2)\dots(n_R-\#_b)]$). As a result of this combinatorial multiplicity, the adsorption curve becomes significantly sharper on varying the receptor coverage (fig. 11(d)) as shown pictorially in fig. 11(e).

5. – Equilibrium clustering

The synthesis of limited-valence colloids in the last years has brought a renewed interest in their clustering process, a topic which had previously been the focus of supramolecular chemistry and polymer physics. The old studies of Flory [126] and Stockmayer [127, 103], despite their mean-field validity, provide useful guidance for predicting the aggregation properties of limited-valence colloids and their thermodynamics. It is not surprising, indeed, that the Wertheim theory [104], which has been extensively used in recent years to deepen our understanding of the phase behavior of several patchy colloidal systems [77, 105, 128], assumes loop-less clusters, *e.g.* the same hypothesis of Flory and Stockmayer [129]. The study of the clustering process provides another important example of the role of entropy in controlling the self-assembly of limited-valence colloids.

It is quite instructive to predict the cluster size distribution for a system of N bi-functional patchy particles dispersed in a volume V , knowing that these particles have formed exactly P bonds. For particles with valence two, the possible clusters are chains of variable length n . Then, assuming that the different chains do not interact, the configurational part of the partition function of the system can be written as the product of the partition functions of the individual clusters Q_n , each of them normalised by an $N_n!$ term which accounts for permutations of identical clusters [130, 131]

$$Q = e^{-\beta P \mathcal{F}_b} \prod_n \frac{Q_n^{N_n}}{N_n!}, \quad \text{with } Q_n = \frac{\Omega_n V}{n!},$$

where \mathcal{F}_b is the free energy associated to the existence of one bond, Ω_n indicates the number of ways n distinct particles, each with two distinct reactive sites, can be joined into a chain of length n . The volume term V , expressed in units of the cube of the thermal length, accounts for the cluster center-of-mass entropy. Considering that the first patch in the chain can be selected in $2n$ ways, that the bonded patch of the second particle can be selected in $2(n-1)$ ways and so on, one finds $\Omega_n = 2^n n! / 2$, where the 2 in the denominator accounts for the over-counting since the same chain can be assembled starting from the two distinct ends. As a result,

$$(33) \quad Q = e^{-\beta P \mathcal{F}_b} 2^P \prod_n V^{N_n} / N_n!.$$

Apart from the constant contribution associated to the presence of P bonds, $e^{-\beta P \mathcal{F}_b}$, the remaining free-energy contribution ($-k_B T \ln Q$) is purely entropic and coincides (apart from the trivial constant term $P \ln(2)$) with the one of an ideal gas of chains distributed according to N_n ,

$$(34) \quad \frac{S}{k_B} = P \ln(2) + \sum_{n=1}^{\infty} N_n \left\{ 1 - \ln \frac{N_n}{V} \right\}.$$

The solution for the most probable distribution of chain lengths N_n can now be calculated by requiring that entropy assumes the largest possible value, but satisfying the two constraints in the problem: the conservation of the number of particles ($\sum_{n=1}^{\infty} n N_n = N$) and the total number of bonds. Since each chain of length n has $n - 1$ bonds, the constraint on the number of bonds can be formulated as $\sum_{n=1}^{\infty} (n - 1) N_n = P$.

Defining $\ln \alpha$ and $\ln \beta$ as the Lagrange multipliers associated to the two constraints, the maximization of the entropy S with respect to N_n , including the contribution arising from the Lagrange multipliers, gives

$$(35) \quad \frac{dS}{dN_n} = \left(1 - \ln \frac{N_n}{V} \right) - 1 + n \ln \alpha + (n - 1) \ln \beta = \ln \left[\frac{V}{N_n} \alpha^n \beta^{n-1} \right] = 0$$

or equivalently

$$(36) \quad \frac{N_n}{V} = \alpha (\alpha \beta)^{n-1}.$$

Plugging this result in the equations defining the two constraints, it is possible to calculate the exact values of α and β . In terms of fraction of formed bonds $p_b = P/N$, one finds $\alpha \beta = p_b$ and $\alpha = \frac{N}{V} (1 - p_b^2)$, such that

$$(37) \quad N_n = \alpha (\alpha \beta)^{n-1} = N (1 - p_b^2) p_b^{n-1}.$$

The equilibrium cluster size distribution N_n is thus exponential, a well known result of equilibrium polymerization [35]. The result can also be easily interpreted as a chain with two open bonds at the ends $((1 - p_b)^2)$ times $n - 1$ bonds between the n particles (p_b^{n-1}).

If the colloidal particles can form f bonds, the same method can be applied to evaluate the cluster size distribution. The function Ω_n is more complex than for the $f = 2$ case and can be easily calculated only for very small n . The resulting expression for generic f , first derived by Stockmayer [127], is

$$(38) \quad \Omega_n = \frac{f^n (fn - n)!}{(fn - 2n + 2)!}$$

and the corresponding cluster size distribution is [127]

$$(39) \quad N_n = N \frac{\Omega_n}{n!} (1 - p_b)^f [p_b (1 - p_b)^{f-2}]^{n-1}.$$

This expression predicts that when p_b reaches the value $p_b = 1/(f - 1)$, the clusters size distribution N_n becomes a power law in n with exponent -2.5 , indicating the presence of a percolation (infinite cluster) transition.

Despite the hypothesis of absence of loops in finite-size clusters, the Flory-Stockmayer predictions quite accurately describe clustering in limited-valence colloids, the agreement increasing on decreasing f [128, 132].

6. – When entropy competes with energy

Energy-entropy competition is at the heart of several very important self-assembly processes in soft-matter systems (and in atomic and molecular systems too [133]). It beautifully manifests itself in the emergence of structures controlled by energy competing with structures stabilized by entropy. The possibility to exploit all the different forms of entropy previously discussed can indeed lead to the entropic stabilization at intermediate temperatures of local or global structures, which then give way on cooling to distinct organizations at low T , where energy becomes the leading driving force.

6.1. Dipolar hard spheres. – The dipolar hard sphere (DHS) model is a paradigm for the self-assembly of anisotropic particles [137] and a challenge for present day theories of fluids. As we will see, in this model, the entropy associated to a network formation competes with the energy promoting chain formation, resulting in significant T -dependent structural changes. The DHS model, a point-dipole at the center of a hard sphere, can be considered as the next simplest modification of the hard-sphere (HS) model, after the point charge one (the restricted primitive model of electrolyte solutions [138, 139]). Thus, it is quite interesting to note that, despite its simplicity, contrasting opinions still exist about its phase behavior and specifically about the existence of a liquid phase distinct from the fluid one (*e.g.* the existence of a gas-liquid critical point). de Gennes and Pincus [140] were the first to point out that, in the dilute limit, one could spherically average the dipolar potential, resulting into an effective isotropic attraction. This could promote a liquid-gas phase separation at low T as in ordinary van der Waals fluids. It was then realized that the highly anisotropic character of the dipole-dipole interaction, which promotes the self-assembly of dipoles into chains, imposes a local order that is significantly different from the one characteristic of simple fluids [141-143]. Consistently, the first computer simulation studies, although plagued by equilibration issues, provided evidence of an extended nose-to-tail chaining and failed to found evidence of a phase transition [144, 145]. The debate on the existence of a critical point in DHS was rejuvenated by additional simulations studies [146, 134, 147] and by a seminal paper by Tlusty and Safran (TS) [136]. A new type of phase transition was postulated, reinforced, rather than weakened, by the chaining process. Despite the most recent numerical studies suggest that the DHS model does not have a gas-liquid critical point [135], the TS theory [136] deserves to be discussed since it provides a beautiful example of energy-entropy competition in soft-matter systems.

The main idea of TS [136] is to describe the DHS fluid not in terms of particles but in terms of a gas of defects. Indeed, as shown by the representative configuration in fig. 12(b-c), particles form quite polydisperse chains of oriented dipoles. On cooling, the average length of these chains (fig. 12(d)) increases and, at the same time, due to the conservation of the total number of particles, the number of polymers decreases. TS propose to consider the number of chain ends as the excitations (or defects) over the $T = 0$ structure, the structure in which all particles belong to one infinite chain. If chain ends were the only defect type, then DHS would behave as a living polymer system and the fluid structure would be described (as discussed in sect. 5) by an exponential distribution of chain lengths, with an average length diverging on approaching $T = 0$.

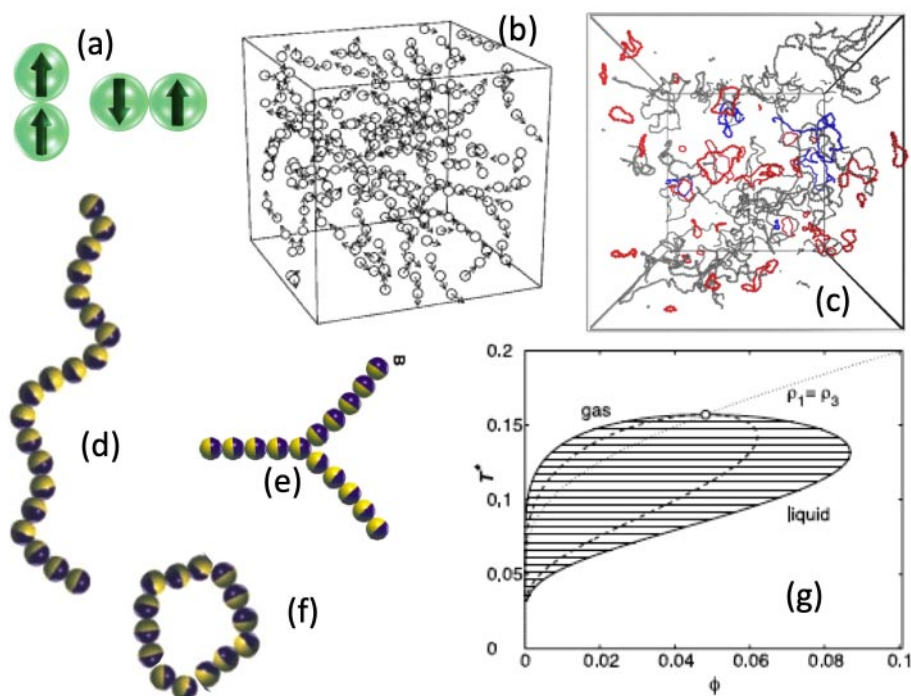


Fig. 12. – Dipolar hard spheres: (a) Cartoon of two dipolar hard spheres in the head-tail configuration and in the antiparallel configuration. (b) Reproduction of one of the first simulations of DHS showing chaining (redrawn from [134]). (c) A typical low-temperature configuration showing the presence of several ring structures (redrawn from [135]). (d) A cartoon of a DHS polymer. (e) A cartoon of the Y junction. (f) A cartoon of a ring structure. (g) The re-entrant phase diagram proposed by TS (redrawn from [136]).

Beside chain ends, TS also identified Y junctions (fig. 12(e)) as possible defects of the chain gas (or, equivalently, as dominant terms in the polymer-polymer interaction). In a Y junction, a polymer end binds to a monomer of another polymer to reduce the system energy. The Y junctions offer the possibility of generating a three-dimensional network of connected chains and therefore a liquid phase. In this model, entropy strongly enters as the quantity controlling the number of distinct Y junctions which can be formed.

In the mean-field TS theory, both the density of chain ends and the density of junctions follow a power law in density with exponents $1/2$ and $3/2$, respectively. These exponents play a major role, controlling the density dependence of the system free energy. Accordingly, as the temperature is lowered, Y junctions and chain ends phase separate in a dense network rich in Y junctions and a dilute gas rich in chain ends. The possibility of such a phase transition, which crucially depends on the number density of topological defects (chain ends and junctions) and their scaling with density, gives rise to a peculiar re-entrant phase diagram, in which the density of the liquid phase approaches the vanishing density of the gas phase on cooling (fig. 12(g)).

The TS model focuses on two types of topological defects of the network, chain ends and branching points (junctions). Recent simulation studies [135] have shown that, at low T and low density, a large fraction of particles organize themselves into rings

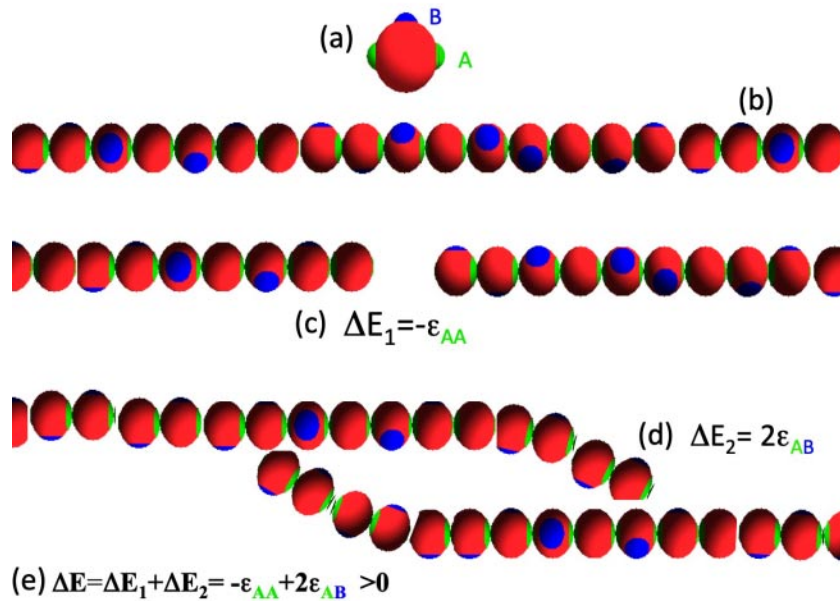


Fig. 13. – Patchy particle model. (a) A colloidal particle is modelled as a hard sphere (red) decorated by two green sites (A), providing chaining, and one blue site (B), providing branching. Only AA and AB bonds are possible. (b) The infinite-chain structure. To evaluate the range of $\epsilon_{AA}/\epsilon_{AB}$ values for which the infinite chain is the ground state, consider the process by which a bond is broken and the two newly created ends are connected with available B sites: to break a bond costs an amount of energy $\Delta E_1 = -\epsilon_{AA}$ (c); the two newly created ends are reconnected via AB bonds (d), with an energetic gain $\Delta E_2 = 2\epsilon_{AB}$. The total energy cost in the process is $\Delta E = \Delta E_1 + \Delta E_2 = -\epsilon_{AA} + 2\epsilon_{AB}$. Thus, $\Delta E > 0$ if $\epsilon_{AB} > \epsilon_{AA}/2$. In this case, the infinite chain is the ground state. In the opposite case, branching becomes more convenient also at $T = 0$ and the ground state is a branched structure.

(fig. 12(f)), a structure which is not considered in the TS assumptions. The possibility for the chain ends to annihilate into the formation of a ring, originating essentially in ground-state finite-size aggregates, is consistent with the numerically observed absence of a gas-liquid critical point [135].

6.2. Competing patches. – Despite the TS model is not appropriate to describe DHS due to the self-assembly of rings (and even more complex structures) at low T [148,149] the assumptions of the TS model become exact for specifically designed competing patchy colloids [150,151]. These are hard colloids with three attractive patches: two A sites and one B site, with AA bonds of energy ϵ_{AA} providing chaining and AB bonds of energy ϵ_{AB} providing branching. As shown in fig. 14, the ground state of this system changes abruptly when $\epsilon_{AB} = 0.5\epsilon_{AA}$.

The free energy of this model can be calculated with the first-order perturbation theory of Wertheim [152,153] and the Flory-Stockmayer theory of polymerization [128,154]. Thus, it is possible to study the criticality of patchy particles from a standard liquid-state theory approach. At low densities and T , the resulting expression is equivalent to the TS theory [155,150].

In Wertheim's approach [152, 153], the free energy of a system with N particles is written as a sum of the reference HS free energy (given by, *e.g.*, the Carnahan-Starling [41] form) and a bonding contribution F_b ,

$$(40) \quad \frac{\beta F_b}{N} = 2 \log X_A + f_B \log X_B - X_A - \frac{f_B}{2} X_B + \frac{1}{2}(2 + f_B),$$

where f_B is the number of B patches in each particle, $\beta \equiv (k_B T)^{-1}$, T is the temperature, and X_A and X_B are, respectively, the fractions of sites A and B which are not engaged in a bond. X_A and X_B can be related to temperature and density through the laws of mass action [150]

$$(41) \quad \begin{cases} X_A + 2\phi\Delta_{AA}X_A^2 + f_B\phi\Delta_{AB}X_AX_B = 1, \\ X_B + 2\phi\Delta_{AB}X_AX_B = 1, \end{cases}$$

where $\phi \equiv v_s \rho$ is the packing fraction, $v_s = \frac{\pi}{6}\sigma^3$ is the particle volume, ρ is the number density, and the quantities $\Delta_{\alpha\beta}$ ($\alpha, \beta = A, B$) are given by

$$(42) \quad \Delta_{\alpha\beta} = \frac{1}{v_s} \int g_{\text{HS}}(\mathbf{r}) [\exp(\beta\epsilon_{\alpha\beta}) - 1] \mathbf{d}\mathbf{r},$$

where $g_{\text{HS}}(\mathbf{r})$ is the HS radial distribution function, and the integral extends over the bonding volume.

Differentiation of the free energy with respect to the volume yields the pressure P . From the T - and ρ -dependences of P , one can locate, by standard methods, the critical point and the liquid-vapour coexistence curve. The resulting phase diagram has the same shape as the one predicted by TS for dipolar HS (fig. 12(g)).

6.3. Janus. – Another soft-matter example of competition between energy and entropy is provided by Janus colloidal particles [156], *i.e.*, particles which attract each other via just one half of their surface (one hemisphere). The phase diagram of the disordered phases has been revealed [157], showing that, at odds with a standard liquid-vapor phase separation, the vapor phase is composed of micelles and vesicles. Particles in these clusters have very precise orientations, allowing them to bind simultaneously with several neighbours, providing a strong energetic driving force which overcomes the standard entropic contribution in favour of a monomer state typical of standard gases. Thus, particles in micelles have a very low energy as compared to the dense liquid phase, which is instead stabilized by the much larger orientational entropy. On further cooling, the entropic stabilization of the dense phase becomes less and less relevant, progressively suppressing the two-phase region.

6.4. Re-entrant gels. – Both previous examples show the importance of being able to design energy-stabilized structures which can act as independent clusters at low temperature. Under these conditions, the low-temperature phase essentially consists of a gas of aggregates interacting via excluded-volume effects. These examples have also shown that if a competing mechanism exists that stabilises a different local structure through entropy, then a different phase can emerge. As a last example of energy-entropy

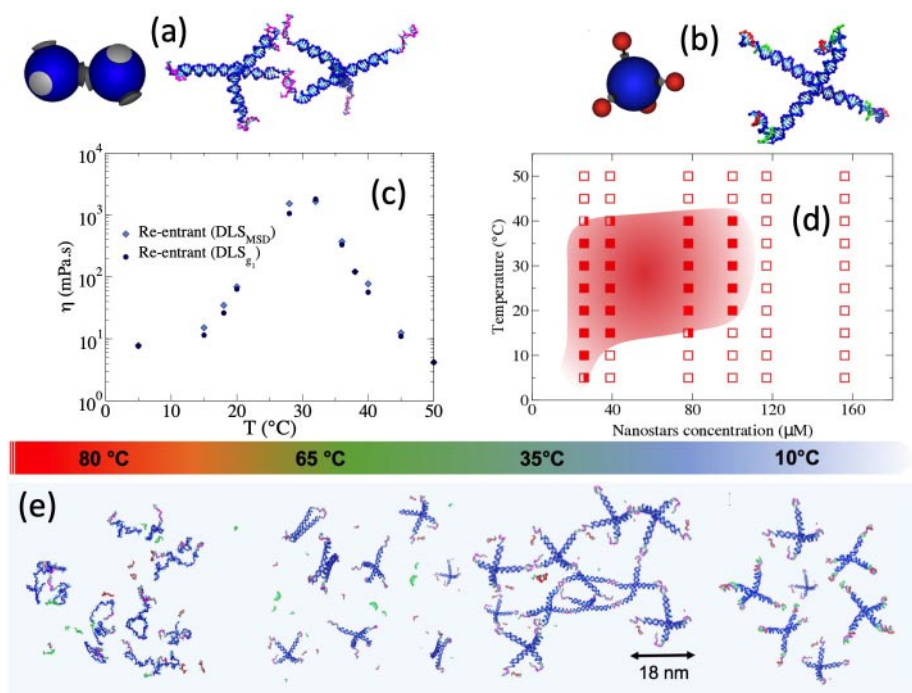


Fig. 14. – Re-entrant DNA gels. (a) Tetravalent patchy particle model and corresponding DNA nanoparticle. An AA bond between two particles, resulting from the association of two complementary DNA single strands, is shown. (b) Tetravalent patchy particle model and corresponding DNA nanoparticle bonded with bond “capping” particles. In the case of the DNA, these capping particles are provided by two single-strand DNA sequences (green and red) complementary to different parts of the A binding sequence. (c) Viscosity measurements as a function of temperature showing the large increase on heating. (d) Phase diagram of the DNA system, showing the Safran-like re-entrant behavior. (e) Cartoon of the structure of the system at different T . At high T all strands are isolated. Around 65°C , the DNA tetravalent nanoparticles are self-assembled. Around $T = 35^\circ\text{C}$, the system forms a gel via AA bonds which then, on further cooling, transforms into a gas of isolated capped nanostars. ((d), redrawn from ref. [158], (c,e) redrawn from ref. [159]).

competition, I discuss here a (stoichiometric) binary mixture of tetravalent (A) and monovalent (B) particles, again with only AA and AB bonds. With an appropriate choice of ϵ_{AA} and ϵ_{AB} , at low T , the system organizes itself into a gas of AB_4 aggregates. With a judicious choice of the bonding entropy, the AB bonds can be made less stable than the AA ones such that, on rising the temperature, AB bonds are progressively substituted with AA ones. When this is the case the system converts upon heating from a fluid of freely diffusing AB_4 aggregates into a tetrafunctional network of A particles coexisting with a gas of B ones (see fig. 14). This system, which is a low-viscosity fluid at low T , progressively transforms into a viscous gel on heating, increasing its viscosity by several orders of magnitude. Recently, such theoretical prediction has been transformed into an experimental realisation [158] by realizing tetra-functional and mono-functional particles completely made of DNA. The experimental results (see fig. 14) confirm that the system exhibits a non-monotonic T dependence of the viscosity, covering about three orders of magnitude.

7. – Conclusions

In this review I have presented several soft-matter systems in which entropy plays a dominant role as driving force favouring self-assembly of ordered structures. I have attempted to clarify that order, in the way it is perceived by us, can correspond to states of maximum entropy. This inevitably calls attention on the importance of always evaluating entropy as the logarithm of the number of microstates concurring to the same macroscopic state. I also hope I have clarified why in soft matter, oppositely to atomic and molecular systems, entropy plays such an important role. Several cases have been explored, starting from the self-assembly of hard colloidal particles, where entropy is by definition the only driving force. We have seen how entropy associated to translational and orientational degrees of freedom—the last arising from particles shape or from anisotropic interactions in otherwise spherical particles— compete and how entropy differently weights fluids, liquid crystals and crystal states. We have also seen how entropy plays an important role in limited-valence particles, under conditions where all possible bonds are formed, *de facto* creating a conceptual link with the self-assembly of hard-body particles.

I have stressed how partial integration of the degrees of freedom associated to apparently irrelevant variables—a process intrinsic in any coarse-graining approach— transforms interactions into free-energy ones. The integrated degrees of freedom often leave their trace into the entropic component. Finally, I have stressed how to exploit combinatorial entropy to design effective interactions with a controllable depth, a necessary condition to avoid kinetic traps or to maximize efficiency in adsorption phenomena. Learning how entropy controls in a subtle way the self-assembly of colloidal particles offers us a handle on how to exploit entropy to direct particle aggregation or to select desired structures.

* * *

The author thanks the organizers of the summer school *SoFun: Soft Matter for Functional Materials*, held in Bordeaux in September 2018, and the organizers of the ICTS school *Entropy, Information and Order in Soft Matter* held in Bangalore in September 2018. This review follows the lecture notes prepared for these two events. The author thanks C. De Michele, E. Lattuada and E. Zaccarelli for their valuable comments and A. Sciortino for a critical reading of the manuscript.

REFERENCES

- [1] ALDER B. and WAINWRIGHT T., *J. Chem. Phys.*, **27** (1957) 1208.
- [2] ONSAGER L., *Ann. New York Acad. Sci.*, **51** (1949) 627.
- [3] GLOTZER S. C. and SOLOMON M. J., *Nat. Mater.*, **6** (2007) 557.
- [4] PAWAR A. B. and KRETZSCHMAR I., *Macromol. Rapid Commun.*, **31** (2010) 150.
- [5] DUGUET E., DÉSSERT A., PERRO A. and RAVAINÉ S., *Chem. Soc. Rev.*, **40** (2011) 941.
- [6] YI G.-R., PINE D. J. and SACANNA S., *J. Phys.: Condens. Matter*, **25** (2013) 193101.
- [7] RAVAINÉ S. and DUGUET E., *Curr. Opin. Colloid Interface Sci.*, **30** (2017) 45.
- [8] BIANCHI E., CAPONE B., COLUZZA I., ROVIGATTI L. and VAN OOSTRUM P. D., *Phys. Chem. Chem. Phys.*, **19** (2017) 19847.
- [9] BIANCHI E., *Patchy colloids: A theoretical and numerical perspective on functionalized units for self-assembly*, in *Frontiers of Nanoscience*, Vol. **13** (Elsevier) 2019, pp. 37–60.
- [10] PAWAR A. B. and KRETZSCHMAR I., *Langmuir*, **24** (2008) 355.
- [11] CHEN Q., BAE S. C. and GRANICK S., *Nature*, **469** (2011) 381.

- [12] WANG Y., WANG Y., BREED D. R., MANOHARAN V. N., FENG L., HOLLINGSWORTH A. D., WECK M. and PINE D. J., *Nature*, **491** (2012) 51.
- [13] SACANNA S., IRVINE W., CHAIKIN P. M. and PINE D. J., *Nature*, **464** (2010) 575.
- [14] GONG Z., HUECKEL T., YI G.-R. and SACANNA S., *Nature*, **550** (2017) 234.
- [15] JO I.-S., LEE S., ZHU J., SHIM T. S. and YI G.-R., *Curr. Opin. Colloid Interface Sci.*, **30** (2017) 97.
- [16] BIFFI S., CERBINO R., BOMBOI F., PARABOSCHI E. M., ASSELTA R., SCIORTINO F. and BELLINI T., *Proc. Natl. Acad. Sci. U.S.A.*, **110** (2013) 15633.
- [17] FENG L., DREYFUS R., SHA R., SEEMAN N. C. and CHAIKIN P. M., *Adv. Mater.*, **25** (2013) 2779.
- [18] CAI J., TOWNSEND J. P., DODSON T. C., HEINEY P. A. and SWEENEY A. M., *Science*, **357** (2017) 564.
- [19] CAI J. and SWEENEY A. M., *ACS Central Sci.*, **4** (2018) 840.
- [20] LIU H., KUMAR S. K. and SCIORTINO F., *J. Chem. Phys.*, **127** (2007) 084902.
- [21] FUSCO D. and CHARBONNEAU P., *Phys. Rev. E*, **88** (2013) 012721.
- [22] LIKOS C., *Riv. Nuovo Cimento*, **37** (2014) 125.
- [23] ASAKURA S. and OOSAWA F., *J. Chem. Phys.*, **22** (1954) 1255.
- [24] FRENKEL D., *Physica A*, **263** (1999) 26.
- [25] LEKKERKERKER H. N. and TUINIER R., *Colloids and the depletion interaction*, Vol. **833** (Springer) 2011.
- [26] DINSMORE A., WARREN P., POON W. and YODH A., *EPL*, **40** (1997) 337.
- [27] DINSMORE A., YODH A. and PINE D., *Nature*, **383** (1996) 239.
- [28] MASON T., *Phys. Rev. E*, **66** (2002) 060402.
- [29] KRAFT D. J., NI R., SMALLENBURG F., HERMES M., YOON K., WEITZ D. A., VAN BLAADEREN A., GROENEWOLD J., DIJKSTRA M. and KEGEL W. K., *Proc. Natl. Acad. Sci. U.S.A.*, **109** (2012) 10787.
- [30] BUZZACCARO S., COLOMBO J., PAROLA A. and PIAZZA R., *Phys. Rev. Lett.*, **105** (2010) 198301.
- [31] GNAN N., ZACCARELLI E. and SCIORTINO F., *Nat. Commun.*, **5** (2014) 3267.
- [32] ZILMAN A., KIEFFER J., MOLINO F., PORTE G. and SAFRAN S., *Phys. Rev. Lett.*, **91** (2003) 015901.
- [33] LIKOS C. N., *Soft Matter*, **2** (2006) 478.
- [34] TANAKA F., *Polymer Physics: Applications to Molecular Association and Thermoreversible Gelation* (Cambridge University Press) 2011.
- [35] RUBINSTEIN M. and COLBY R. H., *Polymer physics*, Vol. **23** (Oxford University Press, New York) 2003.
- [36] FRENKEL D., *Nat. Mater.*, **14** (2014) 9.
- [37] ESCOBEDO F. A., *Soft Matter*, **10** (2014) 8388.
- [38] PIAZZA R., *Soft matter: the stuff that dreams are made of* (Springer Science & Business Media) 2011.
- [39] BATTIMELLI G. and CICCOTTI G., *Eur. Phys. J. H*, **43** (2018) 303.
- [40] PUSEY P. N. and VAN MEGEN W., *Nature*, **320** (1986) 340.
- [41] CARNAHAN N. F. and STARLING K. E., *J. Chem. Phys.*, **51** (1969) 635.
- [42] BOUBLÍK T. and NEZBEDA I., *Collect. Czech. Chem. Commun.*, **51** (1986) 2301.
- [43] HALL K. R., *J. Chem. Phys.*, **57** (1972) 2252.
- [44] FOFFI G., MCCULLAGH G. D., LAWLOR A., ZACCARELLI E., DAWSON K. A., SCIORTINO F., TARTAGLIA P., PINI D. and STELL G., *Phys. Rev. E*, **65** (2002) 031407.
- [45] ISRAELACHVILI J. N., *Intermolecular and surface forces* (Academic Press) 2011.
- [46] BRYANT G., WILLIAMS S. R., QIAN L., SNOOK I., PEREZ E. and PINCET F., *Phys. Rev. E*, **66** (2002) 060501.
- [47] PIAZZA R., BELLINI T. and DEGIORGIO V., *Phys. Rev. Lett.*, **71** (1993) 4267.
- [48] METROPOLIS N., ROSENBLUTH A. W., ROSENBLUTH M. N., TELLER A. H. and TELLER E., *J. Chem. Phys.*, **21** (1953) 1087.
- [49] ALDER B. and WAINWRIGHT T., *Phys. Rev.*, **127** (1962) 359.
- [50] BERNARD E. P., KRAUTH W. and WILSON D. B., *Phys. Rev. E*, **80** (2009) 056704.

- [51] THORNEYWORK A. L., ABBOTT J. L., AARTS D. G. and DULLENS R. P., *Phys. Rev. Lett.*, **118** (2017) 158001.
- [52] BERNARD E. P. and KRAUTH W., *Phys. Rev. Lett.*, **107** (2011) 155704.
- [53] KOSTERLITZ J. M. and THOULESS D. J., *J. Phys. C: Solid State Phys.*, **6** (1973) 1181.
- [54] HALPERIN B. and NELSON D. R., *Phys. Rev. Lett.*, **41** (1978) 121.
- [55] WEBER H., MARX D. and BINDER K., *Phys. Rev. B*, **51** (1995) 14636.
- [56] RUSSO J. and WILDING N. B., *Phys. Rev. Lett.*, **119** (2017) 115702.
- [57] FRENKEL D., LEKKERKERKER H. and STROOBANTS A., *Nature*, **332** (1988) 822.
- [58] SALAMONCZYK M., ZHANG J., PORTALE G., ZHU C., KENTZINGER E., GLEESON J. T., JAKLI A., DE MICHELE C., DHONT J. K., SPRUNT S. *et al.*, *Nat. Commun.*, **7** (2016) 13358.
- [59] DUSSI S. and DIJKSTRA M., *Nat. Commun.*, **7** (2016) 11175.
- [60] BUSHBY R. J. and LOZMAN O. R., *Curr. Opin. Colloid Interface Sci.*, **7** (2002) 343.
- [61] BELLI S., PATTI A., DIJKSTRA M. and VAN ROIJ R., *Phys. Rev. Lett.*, **107** (2011) 148303.
- [62] BORSHCH V., KIM Y.-K., XIANG J., GAO M., JÁKLI A., PANOV V. P., VIJ J. K., IMRIE C. T., TAMBA M.-G., MEHL G. H. *et al.*, *Nat. Commun.*, **4** (2013) 2635.
- [63] GRECO C. and FERRARINI A., *Phys. Rev. Lett.*, **115** (2015) 147801.
- [64] ALLEN M. P., EVANS G. T., FRENKEL D. and MULDER B., *Adv. Chem. Phys.*, **86** (1993) 1.
- [65] ZANCHETTA G., NAKATA M., BUSCAGLIA M., BELLINI T. and CLARK N. A., *Proc. Natl. Acad. Sci. U.S.A.*, **105** (2008) 1111.
- [66] DE MICHELE C., BELLINI T. and SCIORTINO F., *Macromolecules*, **45** (2011) 1090.
- [67] NGUYEN K. T., SCIORTINO F. and DE MICHELE C., *Langmuir*, **30** (2014) 4814.
- [68] MAN W., DONEV A., STILLINGER F. H., SULLIVAN M. T., RUSSEL W. B., HEEGER D., INATI S., TORQUATO S. and CHAIKIN P., *Phys. Rev. Lett.*, **94** (2005) 198001.
- [69] TORQUATO S. and STILLINGER F. H., *Rev. Mod. Phys.*, **82** (2010) 2633.
- [70] DE GRAAF J., VAN ROIJ R. and DIJKSTRA M., *Phys. Rev. Lett.*, **107** (2011) 155501.
- [71] DAMASCENO P. F., ENGEL M. and GLOTZER S. C., *Science*, **337** (2012) 453.
- [72] DONEV A., CISSE I., SACHS D., VARIANO E. A., STILLINGER F. H., CONNELLY R., TORQUATO S. and CHAIKIN P. M., *Science*, **303** (2004) 990.
- [73] VAN ANDERS G., KLOTS A. D., AHMED N. K., ENGEL M. and GLOTZER S. C., *Proc. Natl. Acad. Sci. U.S.A.*, **111** (2014) E4812.
- [74] HARPER E. S., MARSON R. L., ANDERSON J. A., VAN ANDERS G. and GLOTZER S. C., *Soft Matter*, **11** (2015) 7250.
- [75] ESCOBEDO F. A., *J. Chem. Phys.*, **146** (2017) 134508.
- [76] LEE S., TEICH E. G., ENGEL M. and GLOTZER S. C., *Proc. Natl. Acad. Sci. U.S.A.*, **116** (2019) 14843.
- [77] BIANCHI E., LARGO J., TARTAGLIA P., ZACCARELLI E. and SCIORTINO F., *Phys. Rev. Lett.*, **97** (2006) 168301.
- [78] MIRKIN C. A., LETSINGER R. L., MUCIC R. C. and STORHOFF J. J., *Nature*, **382** (1996) 607.
- [79] SMALLENBURG F. and SCIORTINO F., *Nat. Phys.*, **9** (2013) 554.
- [80] SCIORTINO F., GALLO P., TARTAGLIA P. and CHEN S.-H., *Phys. Rev. E*, **54** (1996) 6331.
- [81] WHITELAM S., TAMBLYN I., HAXTON T. K., WIELAND M. B., CHAMPNESS N. R., GARRAHAN J. P. and BETON P. H., *Phys. Rev. X*, **4** (2014) 011044.
- [82] MORENO A., BULDYREV S., LA NAVE E., SAIKA-VOIVOD I., SCIORTINO F., TARTAGLIA P. and ZACCARELLI E., *Phys. Rev. Lett.*, **95** (2005) 157802.
- [83] MORENO A., SAIKA-VOIVOD I., ZACCARELLI E., LA NAVE E., BULDYREV S., TARTAGLIA P. and SCIORTINO F., *J. Chem. Phys.*, **124** (2006) 204509.
- [84] SCIORTINO F., *Eur. Phys. J. B*, **64** (2008) 505.
- [85] BIFFI S., CERBINO R., NAVA G., BOMBOI F., SCIORTINO F. and BELLINI T., *Soft Matter*, **11** (2015) 3132.
- [86] KAUZMANN W., *Chem. Rev.*, **43** (1948) 219.
- [87] NOYA E. G., ZUBIETA I., PINE D. J. and SCIORTINO F., *J. Chem. Phys.*, **151** (2019) 094502.

- [88] ROMANO F., SANZ E. and SCIORTINO F., *J. Chem. Phys.*, **132** (2010) 184501.
- [89] FRENKEL D. and LADD A. J., *J. Chem. Phys.*, **81** (1984) 3188.
- [90] VEGA C., SANZ E., ABASCAL J. and NOYA E., *J. Phys.: Condens. Matter*, **20** (2008) 153101.
- [91] HU H., RUIZ P. S. and NI R., *Phys. Rev. Lett.*, **120** (2018) 048003.
- [92] VAN DER MEULEN S. A. and LEUNISSEN M. E., *J. Am. Chem. Soc.*, **135** (2013) 15129.
- [93] FENG L., PONTANI L.-L., DREYFUS R., CHAIKIN P. and BRUJIC J., *Soft Matter*, **9** (2013) 9816.
- [94] ANGIOLETTI-UBERTI S., VARILLY P., MOGNETTI B. M. and FRENKEL D., *Phys. Rev. Lett.*, **113** (2014) 128303.
- [95] McMULLEN A., HOLMES-CERFON M., SCIORTINO F., GROSBERG A. Y. and BRUJIC J., *Phys. Rev. Lett.*, **121** (2018) 138002.
- [96] ROMANO F. and SCIORTINO F., *Nat. Mater.*, **10** (2011) 171.
- [97] ROMANO F. and SCIORTINO F., *Soft Matter*, **7** (2011) 5799.
- [98] MAO X., CHEN Q. and GRANICK S., *Nat. Mater.*, **12** (2013) 217.
- [99] MONTARNAL D., CAPELOT M., TOURNILHAC F. and LEIBLER L., *Science*, **334** (2011) 965.
- [100] SMALLENBURG F., LEIBLER L. and SCIORTINO F., *Phys. Rev. Lett.*, **111** (2013) 188002.
- [101] BOMBOI F., CAPRARA D., FERNANDEZ-CASTANON J. and SCIORTINO F., *Nanoscale*, **11** (2019) 9691.
- [102] BÖHMER R., NGAI K., ANGELL C. A. and PLAZEK D., *J. Chem. Phys.*, **99** (1993) 4201.
- [103] STOCKMAYER W. H., *J. Polym. Sci.*, **9** (1952) 69.
- [104] WERTHEIM M., *J. Stat. Phys.*, **35** (1984) 19.
- [105] TAVARES J. M., TEIXEIRA P. I. C. and TELO DA GAMA M., *Mol. Phys.*, **107** (2009) 453.
- [106] LU P. J., ZACCARELLI E., CIULLA F., SCHOFIELD A. B., SCIORTINO F. and WEITZ D. A., *Nature*, **453** (2008) 499.
- [107] Vliegenthart G. and Lekkerkerker H. N., *J. Chem. Phys.*, **112** (2000) 5364.
- [108] ANDERSON V. J. and Lekkerkerker H. N., *Nature*, **416** (2002) 811.
- [109] PHAM K. N., PUERTAS A. M., BERGENHOLTZ J., EDELHAARF S. U., MOUSSAID A., PUSEY P. N., SCHOFIELD A. B., CATES M. E., FUCHS M. and POON W. C., *Science*, **296** (2002) 104.
- [110] SCIORTINO F., *Nat. Mater.*, **1** (2002) 145.
- [111] ANZINI P. and PAROLA A., *Soft Matter*, **13** (2017) 5150.
- [112] LIN K.-H., CROCKER J. C., PRASAD V., SCHOFIELD A., WEITZ D. A., LUBENSKY T. and YODH A., *Phys. Rev. Lett.*, **85** (2000) 1770.
- [113] HERTLEIN C., HELDEN L., GAMBASSI A., DIETRICH S. and BECHINGER C., *Nature*, **451** (2008) 172.
- [114] FRANOSCH T., LANG S. and SCHILLING R., *Phys. Rev. Lett.*, **109** (2012) 240601.
- [115] QI W., GANTAPARA A. P. and DIJKSTRA M., *Soft Matter*, **10** (2014) 5449.
- [116] FILALI M., OUAZZANI M. J., MICHEL E., AZNAR R., PORTE G. and APPELL J., *J. Phys. Chem. B*, **105** (2001) 10528.
- [117] NYKYPANCHUK D., MAYE M. M., VAN DER LELIE D. and GANG O., *Nature*, **451** (2008) 549.
- [118] PARK S. Y., LYTTON-JEAN A. K., LEE B., WEIGAND S., SCHATZ G. C. and MIRKIN C. A., *Nature*, **451** (2008) 553.
- [119] WANG Y., WANG Y., ZHENG X., DUCROT É., YODH J. S., WECK M. and PINE D. J., *Nat. Commun.*, **6** (2015) 7253.
- [120] ANGIOLETTI-UBERTI S., MOGNETTI B. M. and FRENKEL D., *Nat. Mater.*, **11** (2012) 518.
- [121] BACHMANN S. J., KOTAR J., PAROLINI L., ŠARIĆ A., CICUTA P., DI MICHELE L. and MOGNETTI B. M., *Soft Matter*, **12** (2016) 7804.
- [122] SCIORTINO F., GANG O. and KUMAR S., submitted (2019).
- [123] ZHANG D. Y. and WINFREE E., *J. Am. Chem. Soc.*, **131** (2009) 17303.
- [124] MARTINEZ-VERACOECHEA F. J. and FRENKEL D., *Proc. Natl. Acad. Sci. U.S.A.*, **108** (2011) 10963.

- [125] KITOV P. I. and BUNDLE D. R., *J. Am. Chem. Soc.*, **125** (2003) 16271.
- [126] FLORY P. J., *Principles of polymer chemistry* (Cornell University Press) 1953.
- [127] STOCKMAYER W. H., *J. Chem. Phys.*, **11** (1943) 45.
- [128] BIANCHI E., TARTAGLIA P., LA NAVE E. and SCIORTINO F., *J. Phys. Chem. B*, **111** (2007) 11765.
- [129] BIANCHI E., TARTAGLIA P., ZACCARELLI E. and SCIORTINO F., *J. Chem. Phys.*, **128** (2008) 144504.
- [130] HILL T. L., *An introduction to statistical thermodynamics* (Courier Corporation) 1986.
- [131] SCIORTINO F., *Basic concepts in self assembly*, in *Soft Matter Self Assembly*, Vol. **193** (IOS Press) 2016, p. 1.
- [132] RUSSO J., TARTAGLIA P. and SCIORTINO F., *J. Chem. Phys.*, **131** (2009) 014504.
- [133] WALKER J. S. and VAUSE C. A., *Sci. Am.*, **256** (1987) 98.
- [134] CAMP P. J., SHELLEY J. C. and PATEY G. N., *Phys. Rev. Lett.*, **84** (2000) 115.
- [135] ROVIGATTI L., RUSSO J. and SCIORTINO F., *Phys. Rev. Lett.*, **107** (2011) 237801.
- [136] TLUSTY T. and SAFRAN S., *Science*, **290** (2000) 1328.
- [137] DUDOWICZ J., FREED K. F. and DOUGLAS J. F., *J. Chem. Phys.*, **111** (1999) 7116.
- [138] STELL G., WU K. and LARSEN B., *Phys. Rev. Lett.*, **37** (1976) 1369.
- [139] PANAGIOTOPOULOS A. Z., *J. Chem. Phys.*, **116** (2002) 3007.
- [140] DE GENNES P. G. and PINCUS P. A., *Phys. Kondens. Materie*, **11** (1970) 189.
- [141] VAN ROIJ R., *Phys. Rev. Lett.*, **76** (1996) 3348.
- [142] SEAR R. P., *Phys. Rev. Lett.*, **76** (1996) 2310.
- [143] TEIXEIRA P. I. C., TAVARES J. M. and TELO DA GAMA M. M., *J. Phys.: Condens. Matter*, **12** (2000) 411.
- [144] WEIS J. J. and LEVESQUE D., *Phys. Rev. Lett.*, **71** (1993) 2729.
- [145] VAN LEEUWEN M. E. and SMIT B., *Phys. Rev. Lett.*, **71** (1993) 3991.
- [146] CAILLOL J.-M., *J. Chem. Phys.*, **98** (1993) 9835.
- [147] JIA R., BRAUN H. and HENTSCHKE R., *Phys. Rev. E*, **82** (2010) 062501.
- [148] ROVIGATTI L., RUSSO J. and SCIORTINO F., *Soft Matter*, **8** (2012) 6310.
- [149] RONTI M., ROVIGATTI L., TAVARES J. M., IVANOV A. O., KANTOROVICH S. S. and SCIORTINO F., *Soft Matter*, **13** (2017) 7870.
- [150] TAVARES J. M., TEIXEIRA P. I. C. and TELO DA GAMA M. M., *Phys. Rev. E*, **80** (2009) 021506.
- [151] TAVARES J. M., TEIXEIRA P. I. C. and TELO DA GAMA M. M., *Mol. Phys.*, **107** (2009) 453.
- [152] WERTHEIM M., *J. Stat. Phys.*, **35** (1984) 19; 35.
- [153] WERTHEIM M., *J. Stat. Phys.*, **42** (1986) 459; 477.
- [154] TAVARES J. M., TEIXEIRA P. I. C., DA GAMA M. M. T. and SCIORTINO F., *J. Chem. Phys.*, **132** (2010) 234502.
- [155] RUSSO J., TAVARES J. M., TEIXEIRA P. I. C., TELO DA GAMA M. M. and SCIORTINO F., *Phys. Rev. Lett.*, **106** (2011) 085703.
- [156] WALTHER A. and MÜLLER H., *Soft Matter*, **4** (2008) 663.
- [157] SCIORTINO F., GIACOMETTI A. and PASTORE G., *Phys. Rev. Lett.*, **103** (2009) 237801.
- [158] BOMBOI F., ROMANO F., LEO M., FERNANDEZ-CASTANON J., CERBINO R., BELLINI T., BORDI F., FILETICI P. and SCIORTINO F., *Nat. Commun.*, **7** (2016) 13191.
- [159] FERNANDEZ-CASTANON J., BIANCHI S., SAGLIMBENI F., DI LEONARDO R. and SCIORTINO F., *Soft Matter*, **14** (2018) 6431.